



HAL
open science

On the intimate connection between nanoscale adhesion of Yad fimbriae and macroscale attachment of Yad-decorated bacteria to glycosylated, hydrophobic and hydrophilic surfaces.

Gregory Francius, Florian Petit, Eloïse Clément, Yankel Chekli, Jean-Marc Ghigo, Christophe Beloin, Jérôme D.F. Duval

► To cite this version:

Gregory Francius, Florian Petit, Eloïse Clément, Yankel Chekli, Jean-Marc Ghigo, et al.. On the intimate connection between nanoscale adhesion of Yad fimbriae and macroscale attachment of Yad-decorated bacteria to glycosylated, hydrophobic and hydrophilic surfaces.. *Nanoscale*, 2020, 10.1039/D0NR06840C . hal-03053532v1

HAL Id: hal-03053532

<https://hal.univ-lorraine.fr/hal-03053532v1>

Submitted on 11 Dec 2020 (v1), last revised 29 Sep 2021 (v2)

HAL is a multi-disciplinary open access archive for the deposit and dissemination of scientific research documents, whether they are published or not. The documents may come from teaching and research institutions in France or abroad, or from public or private research centers.

L'archive ouverte pluridisciplinaire **HAL**, est destinée au dépôt et à la diffusion de documents scientifiques de niveau recherche, publiés ou non, émanant des établissements d'enseignement et de recherche français ou étrangers, des laboratoires publics ou privés.



Distributed under a Creative Commons Attribution - NonCommercial 4.0 International License

1 **On the intimate connection between nanoscale adhesion of *Yad fimbriae***
2 **and macroscale attachment of *Yad*-decorated bacteria to glycosylated,**
3 **hydrophobic and hydrophilic surfaces**

4
5 Grégory Francius^{1*}, Florian Petit¹, Eloïse Clément¹, Yankel Chekli^{2,3}, Jean-Marc Ghigo²,
6 Christophe Beloin^{2,#}, Jérôme F.L. Duval^{4,#}

7
8
9 ¹ Université de Lorraine, LCPME, UMR 7564, Villers-lès-Nancy, F-54600, France.

10 ² Genetics of Biofilms Laboratory, Institut Pasteur, UMR CNRS2001, Paris, 75015, France.

11 ³ Université de Paris, Sorbonne Paris Cité, Paris, France.

12 ⁴ Université de Lorraine, LIEC, UMR 7360, Vandœuvre-lès-Nancy, F-54501, France.

13
14
15 # equivalent contribution

16
17 * Corresponding authors:

18 gregory.francius@univ-lorraine.fr

22 **Abstract**

View Article Online
DOI: 10.1039/D0NR06840C

23 Yad fimbriae are currently viewed as versatile bacterial adhesins able to significantly mediate
24 host or plant-pathogen recognition and contribute to the persistence of *Escherichia coli* in both
25 the environment and within hosts. To date, however, the underlying adhesion process of Yad
26 fimbriae on surfaces defined by controlled coating chemistries have not been evaluated at the
27 relevant molecular scale. In this work, the interaction forces operational between Yad fimbriae
28 expressed by genetically modified *E. coli* and self-assembled monolayers (SAM) differing in
29 terms of charge, hydrophobicity or nature of decorating sugar units, are quantified by Single
30 Molecule Force Spectroscopy (SMFS) at the nanoscale. It is found that the adhesion of Yad
31 fimbriae onto probes functionalized with xylose is as strong as that measured with probes
32 decorated by anti-Yad antibodies (*ca.* 80 to 300 pN). In contrast, the interactions of Yad with
33 galactose, lactose, mannose, -OH, -NH₂, -COOH and -CH₃ terminated-SAMs are clearly non-
34 specific. Interpretation of SMFS measurements on the basis of Worm-Like-Chain modeling for
35 polypeptide nanomechanics further leads to estimate of the maximal extension of Yad fimbriae
36 upon stretching, that of their persistence length and of their polydispersity. Finally, we evidence
37 for the first time a strong correlation between the adhesion properties of Yad-decorated bacteria
38 addressed from conventional macroscopic counting methods, and the molecular adhesion
39 capacity of Yad fimbriae. Such demonstration advocates for the effort that should be made to
40 understand at the nanoscale level the interactions between fimbriae and their cognate ligands.
41 The results could further help the design of potential anti-adhesive molecules or surfaces to
42 better fight against the virulence of bacterial pathogens.

43

44 **Keywords:**

45 Single molecule force spectroscopy, bacterial adhesion, Yad fimbriae, glycosylated surfaces,
46 Atomic Force Microscopy.

47 **Introduction**

48 Bacterial adhesion and biofilm formation onto biotic and abiotic surfaces are ubiquitous
49 processes that contribute to the adaptation and living of bacteria even under extreme
50 environmental conditions. Since pathogenic bacteria can form biofilms, these processes have
51 become an issue of societal concern and a major challenge in various scientific and applied
52 fields, especially in food and medical industries.¹⁻⁵ For illustration, the ability of some bacteria
53 to adhere onto the surface of fruits or vegetables represents a possible source of foodborne
54 illness and global epidemic outbreak.⁶⁻⁹

55 One of the most recent food-linked outbreak occurred in 2011, when a bacterial epidemics
56 related to enterohemorrhagic *Escherichia coli* (EHEC) strains developed in Germany, then
57 spread to several adjacent countries and ended in a health crisis at the European level.^{10, 11} This
58 epidemic mainly affected children, causing mucous-bloody diarrhea, hemolytic and uremic
59 syndromes, and caused the death of hundreds of people all over Europe.¹² Epidemiological
60 studies evidenced that the lethal infections were caused by an EHEC strain O104:H4^{10, 11} and
61 they hypothesized that the epidemic followed the consumption of contaminated fresh
62 vegetables.¹² These virulent *E. coli* strains belong to a rare serotype defined by its ability to
63 produce shigatoxin (STEC)^{13, 14} and by its facilitated propensity to adhere to digestive mucosa.¹⁵
64 This specific epidemic case pinpointed the importance of adhesion and colonization factors in
65 the success of a pathogen spread.

66 Several studies have demonstrated that bacterial adhesion in the digestive tract is mediated by
67 specific fimbriae or pili located at the bacterial surface.^{16, 17} These fimbriae serve as anchoring
68 bridges to the neighboring environment of the cells and they further contribute to the
69 aggregative adhesion of so-called enteroaggregative *E. coli* (EAEC) strains.^{15, 18, 19} Some of
70 these fimbriae are also known to enhance the virulence of extra-intestinal *E. coli* (EXPEC)
71 strains.²⁰⁻²² Given these contextual elements,²⁰ much work has focused on the identification and

72 characterization of fimbriae composition and structure, as well as on the understanding of their
73 role in adhesion and virulence. Such knowledge is further mandatory for the elaboration of
74 efficient strategies aimed at killing *e.g.* antibiotic resistant cells or at suppressing the adhesion
75 of *e.g.* pathogenic bacteria to surfaces and thereby preventing epidemic risks related to *e.g.* food
76 poisoning.^{23, 24} In that respect, deciphering at the molecular scale the role of fimbriae and of the
77 adhesins positioned at their extremities is urgently needed to address the mechanisms
78 underlying the biomolecular recognition of biotic surfaces and ensuing virulence pattern.

79 Among the so-called chaperone usher family of fimbriae,^{25, 26} the Yad fimbriae are amongst the
80 most prevalent and conserved fimbriae in *E. coli*²⁷ and were demonstrated to modulate bacterial
81 adhesion, biofilm formation and macrophage phagocytosis of different types of *E. coli*.^{28, 29} The
82 Yad fimbriae are composed mostly of YadN major pilin sub-units forming the fimbrial shaft,
83 YadM, YadL, YadK minor pilins and the YadC adhesin displayed at the tip of the fimbriae.³⁰
84 The YadC adhesin is a lectin known for its affinity to xylose³⁰ and for its role in the colonization
85 of corn seed rhizospheres by bacteria.³⁰ D-xylose is obtained from hemicellulose and it is
86 generally found in the composition of leaves and bark of plants but also at the surface of some
87 fruits and vegetables.³¹⁻³³ As *E. coli* including EHEC and UPEC strains can bind to- and form
88 biofilms onto- plants and animal cells, their resistance/tolerance to antibiotic treatments further
89 represents a challenge for the development of non-antibiotic-based therapies.³⁴⁻³⁶ Interestingly,
90 the use of anti-adhesive agents such as globotetraose for P pili or mannosides for type 1 fimbriae
91 is very performant to inhibit bacterial adhesion.^{37, 38} There is therefore much to gain in better
92 understanding how these fimbriae interact with their cognate sugar, and to date, quantitative
93 information on the interaction of Yad fimbriae with xylose remains limited.

94 The purpose of the current work is to address the adhesion of Yad fimbriae-decorated bacteria
95 onto several self-assembled monolayers with various terminal groups (-OH, -CH₃, -COOH, -
96 NH₂) or conjugated to different sugar molecules (D-xylose, D-galactose, D-mannose and D-

View Article Online
DOI: 10.1039/D0NR06840C

Nanoscale Accepted Manuscript

97 lactose), both at the molecular and bacterial population scales. The molecular adhesion of Yad
98 fimbriae to sugar molecules is here retrieved by atomic force spectroscopy operated at the single
99 molecule level (Single Molecule Force Spectroscopy, SMFS for short) with use of dedicated
100 anti-Yad functionalized probe, whereas macroscopic cell adhesion behavior is evaluated by
101 conventional fluorescence-based counting method. The objectives are to i) evidence the
102 existence (or not) of a clear recognition between Yad fimbriae and several model glycosurfaces
103 with controlled surface chemistries, ii) quantify the magnitude of the corresponding molecular
104 interactions forces, and iii) analyze the molecular Yad adhesion features in relation to the
105 macroscopic bacterial adhesion properties. For the sake of comparison, all results pertaining to
106 the adhesion properties of Yad fimbriae and Yad fimbriae-decorated bacteria with respect to
107 sugars and corresponding glycosylated surfaces are systematically set against those obtained
108 from the molecular interactions measured between functionalized AFM probes and
109 macrosurfaces decorated by antibodies that specifically target the YadC and YadN sub-units of
110 the Yad fimbriae. The results allow a classification of the magnitude of the interaction force
111 operational between Yad fimbriae and various surfaces differing in terms of
112 hydrophilic/hydrophobic balance and nature of the sugar units they support. The analysis
113 further unequivocally demonstrates that macroscopic adhesion of Yad-decorated bacteria is
114 dictated by the very molecular adhesion properties of the Yad fimbriae.

115

116 **Materials and methods**

117 **Bacterial strains**

118 The genetic profiles of two *E. coli* K-12 mutant strains used in this study (Δ_{4adh} and
119 Δ_{4adh_PcLyad}) are summarized in **Table 1**. They derived from previously constructed
120 strains.^{30, 39} The isogenic Δ_{4adh_PcLyad} and Δ_{4adh} strains, producing or not Yad fimbriae,
121 respectively, were constructed from *E. coli* MG1655 (*E. coli* genetic stock center CGSC#6300).

122 They carry the *gfpmut3* gene, encoding the Gfp protein, linked to the *bla* ampicillin resistance
123 gene (*amp^R*, 100 µg/mL) as well as a deletion of the *fliE* to *fliR* flagellar genes replaced by the
124 *cat* chloramphenicol resistance gene (*cm^R*, 25 µg/mL). Both strains have been additionally
125 deleted for the *fim* operon encoding type 1 fimbriae (Δ *fimA-H::zeo*, *zeo^R* 50 µg/mL), for the
126 *agn43* gene, encoding the Ag43 auto-aggregating protein, with the Kanamycin resistance
127 encoding gene that has been flipped out using the pCP20 plasmid (Δ *flu::FRT*)⁴⁰ as well as for
128 the *csgA* gene encoding the main component of the curli fimbriae. These two strains are then
129 deleted for the four main adhesins/cell surface appendages of *E. coli* K-12. In *E. coli* K-12, the
130 *yad* fimbrial operon is cryptic.^{30, 41} Then, to evaluate the impact of the production of the Yad
131 fimbriae, we additionally transduced the *kmPcLyad* construction into the Δ *4adh* strain to obtain
132 the Δ *4adh_PcLyad* strain. In this latter strain, the *yad* operon is under control of the lambda P_R
133 promoter and is expressed constitutively.

134

135 **Bacterial growth conditions, and sample preparation for Atomic Force Microscopy** 136 **(AFM) imaging.**

137 Bacteria were pre-grown overnight at 30°C without agitation in M63B1 minimal medium
138 supplemented with 0.4% glucose (M63B1glu) and with the appropriate antibiotics for the
139 proper selection of the strain of interest (**Table 1**). The next day, fresh M63B1glu medium was
140 inoculated with the overnight culture (OD₆₀₀ of *ca.* 0.05) and cultivated under the same
141 conditions until the biomass reached an OD₆₀₀ of 0.5. Then, 200 µL of the bacterial suspension
142 were placed onto NH₂-decorated substrates for 30 minutes, as detailed in the next section. The
143 samples were extensively rinsed with PBS solution to remove M63B1glu, and placed directly
144 into the AFM closed fluid-cell with 2 mL PBS solution.

145

146 **Preparation of Yad antibodies-decorated surfaces, self-assembled monolayers and**

147 **glycosylated surfaces**View Article Online
DOI: 10.1039/D0NR06840C

148 Rabbit polyclonal antibodies against *E. coli* YadC and YadN proteins were generated
149 previously³⁰ and absorbed on whole protein lysates of MG1655_Δ*yad* strain. IgG were then
150 purified and concentrated using the NAb Protein A/G Spin Purification Kit (Thermo Fisher
151 Scientific) and dialyzed against PBS using Slide-A-Lyzer® MINI Dialysis Devices, 10 K
152 MWCO, 0.5 mL (Thermo Fisher Scientific). D-Mannosamine (C₆H₁₁O₅-NH₂), ethanolamine
153 (C₂H₇NO), dimethylsulfoxide (DMSO), triethylamine (C₆H₁₅N), sodium cyanoborohydride
154 (NaCNBH₃), N-(3-Dimethylaminopropyl)-N'-ethylcarbodiimide hydrochloride (EDC), N-
155 hydroxysuccinimide (NHS), 1-dodecanethiols (HS-C₁₁H₂₂-CH₃), 11-Amino-1-undecanethiol
156 hydrochloride (HS-C₁₁H₂₂-NH₂), 12-mercapto-1-undecanoic acid (HS-C₁₁H₂₂-COOH), 11-
157 Mercapto-1-undecanol (HS-C₁₁H₂₂-OH) and PBS tabs were purchased from Sigma-Aldrich
158 (Sigma Aldrich, Saint-Quentin Fallavier, France) and used as received. PEG-acetal linkers were
159 purchased from Hermann Gruber group (Institute of Biophysics, University of Linz, Austria).
160 Gold-coated glass substrates were obtained by means of a sputter coater (Milexia, K575 Turbo
161 Q150T S, France). In detail, the borosilicate substrates (ref. OVM4-0.9514 of 14 mm × 14 mm
162 × 1 mm) were purchased from Preciver (Preciver Activités, Noisy-le-Grand, France) and were
163 coated with a 20 nm thick chromium layer and a topmost 60 nm gold layer. Gold-coated glass
164 slides were subsequently cleaned with chloroform for 10 min, dried with nitrogen, and then
165 placed into a UV-ozone cleaner (PSD UV4, Novascan Technologies Inc. Ames, IA) for 30 min.
166 Substrates with -NH₂, -OH, -CH₃ and -COOH as terminal groups were prepared according to
167 the following procedure. One side of the gold-coated glass slides previously prepared were
168 brought overnight in contact with a solution of alkanethiols (either HS-C₁₁H₂₂-NH₂, HS-C₁₁H₂₂-
169 OH, HS-C₁₁H₂₂-CH₃ or HS-C₁₁H₂₂-COOH) at 1 mM in pure ethanol. Samples were then
170 abundantly rinsed twice with ethanol for 10 min, dried with nitrogen beam and stored in PBS
171 solution at 4°C prior to experiments.

172 Prior to the preparation of the different antibodies and of the glycosylated surfaces of interest
173 in this work, one side of the gold-coated glass slides was brought overnight in contact with a 1
174 mM solution of (HS-C₁₁H₂₂-COOH) with pure ethanol as solvent. Samples were then
175 extensively rinsed, twice, with ethanol for 10 min, dried with nitrogen beam and brought in
176 contact for 30 minutes with a solution of EDC/NHS (50 mg/mL: 20 mg/mL) dissolved in water
177 at pH 5.0 in order to activate the carboxylic sites of the substrates. Then, the samples were
178 directly immersed into a solution containing the amino-sugar (either antibodies, xylosamine
179 (Xyl), mannosamine (Man), galactosamine (Gal), lactosamine (Lac)) dissolved at 1 mg/mL in
180 PBS at pH 5.0 for 2 hours. At the end of this step, substrates were dipped in a PBS solution at
181 pH 8.0 for 10 minutes, and extensively rinsed with milli-Q water, and finally stored in PBS
182 solution at 4°C.

183

184 **Infrared reflection absorption spectroscopy (IRRAS)**

185 IRRAS spectra were recorded in the mid-infrared range with use of a Fourier transform infrared
186 spectrometer Nicolet 8700 apparatus equipped with a KBr beam splitter and a MCT detector.
187 An advanced grazing angle specular reflectance accessory (Pike technologies Inc.) with a fixed
188 incidence angle of 80° was used to acquire spectra of the gold-coated surfaces. The spectral
189 resolution was 4 cm⁻¹ and the accumulation time was 2 min. Compartments containing the
190 detector and the specular reflectance accessory were purged by circulating dry N₂. IR
191 absorbance spectra were obtained between 4000 and 600 cm⁻¹. Note that samples were
192 extensively rinsed with milli-Q water and then dried with dry N₂ *prior* to measurement and
193 introduction in the spectrophotometer. A total of 200 scans were collected for each sample and
194 condition examined.

195

196 **Bacterial adhesion by fluorescence microscopy and bacterial membrane integrity assays.**

197 Bacterial adhesion was determined by counting GFP positive Δ_{adh} and Δ_{adh} PclYad
198 bacteria attached to the functionalized surfaces. Briefly, 1 mL of OD₆₀₀ 0.5 cells were deposited
199 on the different functionalized substrates and left for 2h. Bacterial membrane integrity was
200 assessed with propidium iodide (PI) at 160 μ M concentration in sterile PBS. This allows
201 assessing the toxicity of the tested surface coatings against the cells since PI enters the cells
202 only when their membranes are damaged. The bacteria adhered onto the different functionalized
203 substrates were stained with PI during 20 minutes under dark conditions. Then, the samples
204 were rinsed with sterile PBS buffer solution (pH 7.4) to eliminate the excess of dyes, and then
205 fixed with a solution of glutaraldehyde at 2% in PBS for 30 minutes. Subsequently, samples
206 were set in mounting oil environment. Sets of 10 images per samples with green and red
207 fluorescence emissions were acquired simultaneously with the \times 100 oil immersion objective
208 of an Olympus BX51 microscope equipped with an Olympus XC50 camera. PI and GFP
209 fluorescence were observed simultaneously using fluorescence filter cube U-MWIB3
210 (Olympus, excitation filter: BP 460-495 nm, emission filter: LP 510 nm).

211

212 **AFM-probes functionalization.**

213 AFM-probes were functionalized with amino-sugars (xylosamine (Xyl), mannosamine (Man),
214 galactosamine (Gal), lactosamine (Lac)), anti-YadC or anti-YadN antibodies according to the
215 procedure described elsewhere⁴²⁻⁴⁴ and successfully adopted for the detection and stretching of
216 type 1 fimbriae.⁴⁵ Briefly, silicon nitride tips (MLCT, Bruker Nano AXS, Palaiseau, France,
217 spring constant of about 0.01 nN/nm) were first amino-functionalized according to the protocol
218 detailed elsewhere⁴⁶ and tips modified with amino groups further reacted with PEG linkers
219 carrying benzaldehyde functions. The latter were then directly attached to the amino-sugars or
220 antibodies through their terminal NH₂ group.

221

222 **AFM imaging and single-molecule force spectroscopy (SMFS)**

View Article Online
DOI: 10.1039/D0NR06840C

223 AFM images were recorded with a Bioscope Resolve equipment (Bruker AXS, Palaiseau,
224 France) using PeakForce Tapping mode^{47, 48} to image the biological surfaces of interest under
225 air conditions. Force measurements were carried out with a MFP3D-BIO instrument (Oxford
226 Instruments, Mannheim, Germany). Silicon nitride and gold coated cantilevers of conical shape
227 were purchased from Bruker (MLCT and NPG, Bruker AXS, Palaiseau, France) with spring
228 constants of 0.01 nN/nm and 0.12 nN/nm, respectively. Single molecule force spectroscopy
229 experiments were performed in PBS at pH 7.4 and room temperature.

230 Adhesion forces, conformational characteristics and extension of the Yad fimbriae were
231 measured by recording Force-Volume Images (FVI) consisting of a grid of 32×32 force curves
232 obtained upon approach and subsequent retraction of the chemically-modified AFM probe at
233 pulling rates of $1 \mu\text{m/s}$ (SMFS experiments). For each condition examined, force measurements
234 were performed in triplicate over an area of $5 \mu\text{m} \times 5 \mu\text{m}$ after locating the selected bacteria *via*
235 the Olympus IX 71 inverted microscope that supports the AFM.

236 During SMFS experiments, the Yad fimbriae were detected and stretched upon withdrawal of
237 the chemically-modified AFM probe away from the surface. The obtained force-distance curves
238 were then analyzed on the basis of the Worm Like Chain (WLC) model.^{45, 49} This model is most
239 suitable and most frequently used to describe the extension of polypeptides. Within the
240 framework of this theory, the extension z of the macromolecule is related to the retraction force
241 F_{adh} *via* the following equation:^{50, 51}

$$242 \quad F_{\text{adh}}(z) = -\frac{k_B T}{l_p} \left[\frac{z}{L_c} + 4 \left(1 - \frac{z}{L_c} \right)^{-2} - \frac{1}{4} \right] \quad (1)$$

243 where the persistence length l_p reflects chain stiffness, L_c is the total contour length of the
244 macromolecule and k_B is the Boltzmann constant. All FVI were analyzed automatically with

245 use of a home-made MATLAB program described elsewhere.⁴⁹ It is emphasized that force-
246 distance curve measurements were systematically performed on freshly prepared substrates.

247

248

249 **Results and discussion**

250 **Morphological analysis of bacteria constitutively expressing Yad fimbriae**

251 To gain insight into the cell surface morphology of *E. coli* K-12 producing Yad fimbriae, the
252 strains Δ_4adh and Yad fimbriae-producing Δ_4adh_PcLyad were grown at 30°C without any
253 agitation prior to electrostatic immobilization onto a gold substrate exhibiting -NH₂ terminal
254 groups, and then gently dehydrated before imaging by AFM (**Figure 1** and **Figure S1** in
255 **Supporting Information**). AFM images clearly showed that Δ_4adh_PcLyad bacteria
256 constitutively expressing Yad fimbriae are 2.0-2.5 μm rod-like shaped cells decorated with
257 several 50 to 2000 nm long filamentous structures. In contrast, the Δ_4adh bacteria are devoid of
258 such peripheral structures (**Figures 1-S1**). Accordingly, these filamentous structures should
259 correspond to the Yad fimbriae with a typical tubular structure of about 1-2 μm length and 5-8
260 nm in diameter as roughly determined from horizontal cross-sections profiling. This is
261 consistent with previous observation of Yad fimbriae using transmission electron microscopy.³⁰
262 The thin Yad fimbriae are fragile structures, as judged by the presence of many bundles of
263 broken filaments at the substrate surface (**Figure 1**). These broken fimbriae exhibit an average
264 length ranging from *ca.* 50 nm to 1000 nm and are randomly distributed around individual
265 bacterium. These observations related to the fragility of Yad fimbriae are probably the result of
266 structure cracking during the required rinsing step of the sample. Due to the inherent dynamics
267 of fimbriae structures and technical limitation of the used AFM, Yad filaments could not be
268 observed in liquid medium.

269

270 **IRRAS analysis of the model self-assembled monolayers terminated with -NH₂, -OH, -**
271 **CH₃, -COOH, anti-Yad antibodies or sugars (mannose, lactose, galactose and xylose)**

272 Prior to investigation of the impact of chemical coatings on the adhesion properties of Δ_{4adh}
273 and Δ_{4adh} _PcLyad cells, the surface chemistry of the different self-assembled monolayers
274 formed onto the gold-coated substrates was verified by IRRAS (**Figure S2**). The IRRAS spectra
275 of the model substrates obtained by simple adsorption of HS-C₁₁H₂₂-NH₂ (SAM-NH₂), HS-
276 C₁₁H₂₂-OH (SAM-OH), HS-C₁₁H₂₂-CH₃ (SAM-CH₃) and HS-C₁₁H₂₂-COOH (SAM-COOH)
277 show typical absorption bands from the alkyl chain identified at 2950, 2922, 2850, 1450 and
278 1065 cm⁻¹, respectively for the C-H and C-C bonds. The different terminal groups were clearly
279 evidenced by the typical absorption bands at 3395, 3250 and 1550 cm⁻¹ for -NH₂, at 3500 and
280 1080 cm⁻¹ for -OH, and at 17450 cm⁻¹ for -COOH.

281 Concerning the glycosurfaces of interest in this work (SAM-Xylose, SAM-Mannose, SAM-
282 Galactose and SAM-Lactose), their corresponding IRRAS spectra (**Figure S2**) show absorption
283 bands from mannosylated residue at 1510, 1425, 1342, 1267 and 1083 cm⁻¹, from lactosyl at
284 1435, 1382, 1265, 1163 and 1077 cm⁻¹, from galactosyl at 1571, 1470, 1388, 1218 and 1161
285 cm⁻¹ and from xylosyl at 1461, 1365, 1314, 1282 and 1081 cm⁻¹.^{52, 53} The IRRAS spectra of
286 substrates covered by a monolayer of anti-YadC and anti-YadN antibodies feature absorption
287 bands of the proteins at 1653, 1546, 1745 and 1269 cm⁻¹, respectively assigned to amide I,
288 amide II bands, ester groups (C=O) and ν (C-N) bond. Altogether, the chemical surface analyses
289 confirmed the presence of controlled molecular monolayers at the surface of the different gold
290 substrates and, consequently, they support the success of the functionalization procedure we
291 followed.

292

293 **Influence of the substrate chemistry on the macroscopic adhesion of *E. coli* cells producing**
294 **or not the Yad fimbriae.**

295 In order to evaluate how the surface chemistry of the various self-assembled monolayers (SAM) View Article Online
DOI: 10.1039/D0NR06840C
296 determine bacterial adhesion, we incubated the different substrates with defining IRRAS
297 spectra given in **Figure S2** in suspension of GFP fluorescent *E. coli* Δ_{4adh} and Δ_{4adh} _PcLyad
298 cells during 2 hours. Then, after rinsing, samples were stained with the propidium iodide
299 viability dye to assess the toxicity of the functionalized surfaces. Adhered bacteria onto the
300 different substrates were counted upon analysis of attached GFP+ bacterial cells (**Figure 2a**).
301 For the sake of completeness, **Figure S3** and **Figure S4** report characteristic epifluorescence
302 images recorded for the two *E. coli* strains on the surface of the various substrates selected in
303 this work. None of the surface appeared to display any significant toxicity as shown by the
304 absence of, or low level of PI red fluorescence of the cells attached to the different surfaces
305 (**Figure S3** and **Figure S4**). Consistently with the fact that, unlike Δ_{4adh} cells, the
306 Δ_{4adh} _PcLyad cells produce the Yad fimbriae, the results evidence that the amount of
307 Δ_{4adh} _PcLyad cells adhered at the substrates covered by the anti-YadC and anti-YadN
308 antibodies is significantly higher, by *ca.* three orders of magnitude, than that for Δ_{4adh} cells. In
309 detail, the estimated surface concentrations of adhered Δ_{4adh} and Δ_{4adh} _PcLyad are $4\text{-}5\times 10^4$
310 and $2\text{-}4\times 10^7$ cells/cm², respectively, for the anti-YadC and anti-YadN substrates. A similar
311 result is obtained regarding the amount of adhered Δ_{4adh} and Δ_{4adh} _PcLyad cells onto the
312 glycosubstrate with xylose (Xyl) coating, with surface concentrations of adhered Δ_{4adh} and
313 Δ_{4adh} _PcLyad of *ca.* $(5.4\pm 1.3)\times 10^4$ and $(2.4\pm 0.7)\times 10^7$ cells/cm², respectively. This finding is
314 consistent with the specific binding of the YadC tip adhesin to xylose.³⁰ Results pertaining to
315 the adhesion of Δ_{4adh} and Δ_{4adh} _PcLyad cells onto the glycosubstrates with Galactose (Gal),
316 Mannose (Man) and Lactose (Lac) coatings reveal that, here again, cells expressing Yad
317 fimbriae exhibit stronger adhesion properties, *albeit* with a difference for these 3
318 glycosubstrates that is far lesser marked than that discussed for surfaces covered by anti-Yad
319 antibodies and Xylose. Quantitatively, the ratio Δ_{4adh} _PcLyad and Δ_{4adh} cells surface

320 concentrations now amounts to *ca.* 2-4 on SAM-Gal, SAM-Man and SAM-Lac, to be compared
321 with the 650-1000 ratio for substrates covered with Xyl or anti-Yad antibodies.

322 Adhesion of *E. coli* Δ_4adh and Δ_4adh_PcLyad cells on substrates covered by self-assembled
323 monolayers (SAM) terminated by $-NH_2$, $-COOH$, $-OH$ and $-CH_3$ groups was also evaluated in
324 order to address the impact of surface charge and hydrophilic/hydrophobic balance on cell
325 adhesion features. [A detailed analysis of the electrostatic features of the substrates adopted in
326 this work could be performed on the basis of streaming-potential/current measurements and
327 proper interpretation thereof with inclusion of ionic surface conduction if relevant,⁵⁴ or on the
328 basis of chemical force spectroscopy data.⁵⁵ Within the scope of the current work, it is sufficient
329 to state that given the typical dissociation properties of carboxylic and amine groups and
330 considering the pH condition of interest for our SMFS measurements, the surface charge of
331 SAM- \$NH_2\$ and SAM- \$COOH\$ is positive and negative at pH 7.4, respectively, while SAM- \$OH\$
332 and SAM- \$CH_3\$ groups are known to be hydrophilic and hydrophobic surfaces, respectively. The
333 results for SAM- \$OH\$ substrates \(**Figure 2a**\) indicate that surface of \$\Delta_4adh_PcLyad\$ cells is much
334 more hydrophilic than that of \$\Delta_4adh\$ cells \(surface concentrations of \$\(1.8\pm 0.4\)\times 10^6\$ and
335 \$\(6.1\pm 2.2\)\times 10^4\$ cells/cm², respectively\), which is confirmed by the data collected on SAM- \$CH_3\$
336 evidencing a \$\Delta_4adh_PcLyad\$ cells surface hydrophobicity that is significantly lower than for
337 \$\Delta_4adh\$ cells \(surface concentrations of \$\(6.1\pm 2.2\)\times 10^4\$ and \$\(1.1\pm 0.3\)\times 10^6\$ cells/cm², respectively\).](#)

338 Analysis of cell adhesion onto SAM- NH_2 and SAM- $COOH$ substrates further highlights that
339 the affinity of Δ_4adh cells for positively charged surfaces is *ca.* 10 times higher than that of
340 Δ_4adh_PcLyad cells, whereas both cells exhibit similar adhesion properties onto negatively
341 charged substrate (SAM- $COOH$). Last, the affinity of Δ_4adh and Δ_4adh_PcLyad cells for
342 positively charged surfaces is significantly higher (by a factor of *ca.* 20) than that for negatively
343 charged substrates, in agreement with the sign of bacterial surface charge and the well-
344 documented role of electrostatics on cell adhesion.^{56, 57} The results detailed above are converted

345 into percentage of surface coverage by the bacteria (**Figure 2b**), which offers another
346 representation of the respective adhesion properties of Δ_4adh and Δ_4adh_PcLyad cells discussed
347 above for the various substrates considered in this work. For the surface coverage computation,
348 the required uncovered surface area was evaluated with use of standard image-analysis
349 procedure implemented in MATLABTM. Between 24% and 43% of the total initial amount of
350 Δ_4adh_PcLyad bacteria could adhere onto the substrates covered by Xyl and antibodies, which
351 corresponds to only 5-15% surface coverage. As far as the glycosubstrates and the other SAM-
352 OH, SAM-NH₂, SAM-CH₃ and SAM-COOH surfaces are concerned, less than 1% of the total
353 amount of initially incubated Δ_4adh_PcLyad bacteria adhered on the surface substrate, which
354 amounts a surface coverage of less than 0.5%. These results clearly demonstrate a high affinity
355 of Δ_4adh_PcLyad cells to substrates covered with Xyl or antibodies. Conversely, less than 3%
356 of the total initial amount of Δ_4adh bacteria could adhere onto the substrate regardless of their
357 surface chemistry, with a corresponding surface coverage lower than 0.5%. Altogether, our
358 results clearly confirm that the adhesion of Δ_4adh_PcLyad to surfaces functionalized with Xyl
359 and anti-Yad antibodies is specific and mediated by the Yad fimbriae. The developments below
360 provide a molecular insight into this specificity of the interactions between Yad fimbriae and
361 Xyl (or antibodies).

362

363 **Deciphering the interactions between Yad fimbriae, antibodies and glycosyl residues at**
364 **the molecular scale.**

365 We performed single-molecule force spectroscopy measurements (SMFS) on Yad fimbriae
366 exposed at the cell surface of living cells in order to quantify the interaction forces of Yad
367 fimbriae with the glycosyl residues (Xyl, Man, Gal, Lac) or with the specific polyclonal
368 antibodies (anti-YadC and anti-YadN). The latter allow the detection and specific targeting of
369 YadC and YadN pilin constituting the tubular structure of the Yad fimbriae, with YadN being

370 the main constituent of the Yad filamentous structure and YadC being the adhesin located at
371 the tip of the Yad fimbriae. Typical force curves recorded on Δ_{4adh_PcLyad} and Δ_{4adh} bacteria
372 with the different functionalized AFM-probes are reported in **Figure 3** and **Figure S5**,
373 respectively.

374 Unlike typical force curves reported in literature for several types of fimbriae (*e.g.* type 1, F1C,
375 type 3, CFA/I), those obtained for Yad fimbriae are not defined by the succession of regimes
376 that feature a plateau where the force remains constant upon increasing the separation distance
377 between the AFM and the (elongated) structure.^{45, 58-60} The presence of such a plateau for type
378 1 fimbriae is the signature of a tensed helical structure where the FimA sub-units conserve their
379 conformation.^{45, 61} Here, SMFS measurements do not reveal the occurrence of force plateau
380 regime(s) but, instead, they evidence abrupt rupture events between segments of the Yad
381 fimbriae structure and the molecules grafted on the AFM probe, as reflected by the discrete and
382 successive drops of the force with pulling on Yad fimbriae. These findings demonstrate that the
383 YadN sub-units constituting the helical structure of the Yad fimbriae do not retain their
384 conformation when withdrawing the AFM probe from the cell wall but, instead, they are
385 unfolded concomitantly to the stretching of the overall Yad fimbrial structure.

386 Starting the discussion with Δ_{4adh_PcLyad} cells, it is found that 87% to 98% of the force curves
387 recorded with use of AFM-probes functionalized by anti-YadC, anti-YadN and Xyl exhibits at
388 least one adhesive event. This finding contrasts with the 15% to 23% of the force curves for
389 which at least one adhesive event is detected between Yad fimbriae and AFM-probe with the
390 glycosyl functionalities Man, Gal and Lac (**Table 2**). Conversely, less than 5% of the force
391 curves collected between Δ_{4adh} cells surface and AFM-probe contains the signature of -at least-
392 one adhesive event and this conclusion holds for all probe functionalities tested, which includes
393 the AFM- tip modified with YadC- and YadN- antibodies (see **Table 3**). Stated differently, the
394 cell wall of Δ_{4adh} cells interacts poorly with the various molecules grafted at the apex of the

395 AFM-probes. Unlike Δ_{4adh} cells, a significant number of interactions take place between the
396 bacterial cell wall of Δ_{4adh_PcLyad} cells and the different molecules grafted at the end of the
397 AFM-probes, especially Xyl and, obviously, anti-Yad antibodies. These interactions should
398 therefore be attributed to Yad fimbriae. The occurrence of weak interactions between
399 Δ_{4adh_PcLyad} cells with the substrates covered by sugar molecules other than xylose or by the
400 functional groups -OH, -NH₂, -CH₃ and -COOH could originate from non-specific interactions.
401 Indeed, other sub-units of the Yad fimbriae (YadK, YadL, YadM and YadN) could interact in
402 a non-specific manner with these functional groups leading to a weak but measurable adhesion.
403 This result has been already reported for type 1 fimbriae whose terminal sub-unit FimH adhesin
404 that binds specifically to mannose also contributes to the adhesion onto abiotic surfaces through
405 nonspecific interactions.⁶² For the sake of clarity, we stress that the only force curves with one
406 or several adhesive events (*i.e.* those carried out for Δ_{4adh_PcLyad} cells) were subjected to
407 modelling on the basis of eq 1, and the other force curves are therefore not considered in the
408 following modelling developments and related discussion.

409 The force curves carried out on Δ_{4adh_PcLyad} cells are generally defined by a saw tooth pattern
410 with one or several peaks that reflect the adhesive events, irrespective of the nature of the
411 considered AFM-probe (**Figure 3**). These peaks translate the molecular elongation of the Yad
412 fimbriae upon withdrawal of the AFM-probe and the subsequent rupture of the fimbriae-probe
413 as marked by an abrupt decrease of the measured force. The presence of successive adhesive
414 events (and related force maxima) is simply connected to the possible anchoring of the
415 molecules-functionalized AFM probe with several Yad fimbriae defined by various lengths, as
416 previously discussed (**Figures 1 and S1**) and by successive adhesive/rupture events due to the
417 unspooling along the backbone of a single fimbria. **Figure 3** evidences that the elongation of
418 Yad fimbriae structures takes place up to *ca.* 1200-3000 nm distance depending on the
419 chemistry of the AFM probe, which excludes any contribution of the AFM-probe linkers (with

420 length of 6.3 nm in fully extended configuration) to detected adhesion/rupture events. The
421 connection between the occurrence of adhesive events revealed by SMFS and the presence of
422 Yad fimbriae for Δ_4adh_PcLyad cells is supported by the negative control SMFS measurements
423 performed on Δ_4adh bacteria that do not express Yad fimbriae nor any other external structures
424 at their surface: force curves measured for Δ_4adh cells are indeed systematically flat, regardless
425 of the tested functionalities of the AFM probe (**Figure S5**).

426 The analysis of the whole set of force curves collected by SMFS (this set represents *ca.* 5000
427 to 8000 forces curves depending on the tested condition, see details in **Table 2**), makes it
428 possible the determination of the statistic distribution of the number of detected adhesive events
429 as a function of the molecular functionality of the AFM-probe (**Figure S6**), as well as that
430 pertaining to the magnitude of the measured adhesion forces (**Figure 4**) whose averaged values
431 are given in **Table 2** for the various interaction configurations tested. For the AFM-probe
432 functionalized with polyclonal antibodies (anti-YadC and anti-YadN), a monomodal
433 distribution of the number of adhesive events was observed with an average of about 3-4
434 adhesive events per force curve (**Figure S6**). However, the distribution of the magnitude of the
435 corresponding adhesion forces does not display a single maximum but, instead, is multimodal
436 (**Figure 4**). Most (~ 65%) of the adhesive events correspond to 75-200 pN adhesion force
437 amplitude while others are associated to forces in the 200-400 pN range (**Figure 4**). Concerning
438 SMFS results pertaining to AFM-probe functionalized with xylosyl, a bimodal distribution of
439 the number of adhesive events is clearly observed, with a first population of about 3-4 adhesive
440 events per force curve and a second one with *ca.* 8-12 adhesive events in average (**Figure S6**).

441 We find that most (~ 65%) of these adhesive events correspond to the two modes of the
442 distribution of adhesion forces, at about 75 pN and 160 pN, while the others are distributed over
443 the 200-400 pN force range (**Figure 4**). The range of adhesion force achieved with the Yad

444 fimbriae-anti-YadC,N and Xylose pairs is strikingly comparable to that reported for type 1
445 fimbriae-mannosylated surface (adhesion force up to 400 pN).⁴⁵
446 The SMFS measurements performed with the AFM-probes functionalized with mannosyl,
447 galactosyl and lactosyl residues reveal similar patterns with a monomodal distribution of about
448 3-4 adhesive events per force curve (**Figure S6**). In addition, about 80% of these adhesive
449 events are defined by adhesion forces of 50-75 pN and the other events are distributed over
450 force amplitudes covering the 75 to 200 pN range (**Figure 4**). Altogether, the analysis evidences
451 that the interactions between Yad fimbriae and polyclonal antibodies (anti-YadC and anti-
452 YadN) or xylosyl residue grafted at the apex of the AFM-probes are stronger and much more
453 frequent than those taking place between Yad and the other glycosyl residues selected in this
454 work (**Table 2**). In addition, there is no significant difference between the adhesion force
455 measured between Yad fimbriae and anti-YadC, anti-YadN or Xyl-covered surfaces. This
456 finding supports the specific nature of the Yad fimbriae-antibodies and Yad fimbriae-Xyl
457 interactions, which is consistent with the conclusions derived on the basis of cell adhesion
458 properties addressed at the macroscopic scale (**Figure 2**).

459 460 **Assessment of Yad fimbriae nanomechanical features from Worm-Like-Chain modeling.**

461 The SMFS force curves reported in **Figure 3** were interpreted on the basis of the Worm like
462 Chain (WLC) model (eq 1). The theoretical reconstruction of the saw tooth like dependence of
463 the force on separation distance leads to the evaluation of the statistical distribution of three key
464 parameters pertaining to the structural properties of Yad fimbriae, namely: their contour length
465 L_c or, equivalently, their maximal extension/stretching upon withdrawal of the functionalized
466 AFM-probe (**Figure 5**), their molecular periodicity (or peak-to-peak distance) that refers to the
467 distance separating two successive adhesive events taking place along a single fimbria
468 backbone or between the AFM probe and molecules belonging to different Yad fimbriae

469 **(Figure 6)**, and their persistence length which basically refers to the dimension of the shortest
470 Yad fimbriae units behaving as rigid rod **(Figure S7)**. Comparison between the obtained
471 persistence length and size of the YadN subunit **(Table 4)** qualitatively reflects the flexibility
472 of these polymeric subunits of the Yad fimbriae under stretching conditions. For completeness,
473 **Table 2** collects the average values of the maxima of the aforementioned distributions in
474 contour length, persistence length and peak-to-peak separation distance.

475 The SMFS measurements performed with AFM probes defined by antibodies (anti-YadC and
476 anti-YadN) functionalities grafted at their apex allow the specific targeting and pulling on YadC
477 and YadN sub-units of the Yad fimbriae **(Figure 7)**. The contour length retrieved from analysis
478 of the corresponding force curves is distributed over a wide range spanning from a few
479 nanometers to 2000 nm **(Figure 5)**, which obviously renders difficult a clear Gaussian-based
480 assignment of the various modes that define the distribution. Distributions fitting to multimodal
481 Gaussian components should therefore be considered at a qualitative level. Despite of this
482 difficulty, inherent to the SMFS analysis of molecular structures polydisperse in size, two
483 distributions of the contour length of Yad fimbriae stretched by anti-YadN-decorated AFM-
484 probe can be defined: one centered at 247 nm and the other at 761 nm. With using anti-YadC
485 AFM probe, the distributions are clearly shifted to higher values of the contour length, with the
486 possible assignment of three main modes at 936, 1234 and 1648 nm. Assuming that anti-YadC
487 AFM-probe unspools the subunits constituting the fimbriae from the very top end of the Yad
488 structure **(Figure 7)**, the three distributions observed for the contour length suggest the presence
489 of Yad fimbriae whose most frequently encountered dimensions correspond to the maxima of
490 the detected distributions. If complete unspooling of the backbone of the fimbriae takes place,
491 it implies that the probed Yad fimbriae are composed of *ca.* 120, 158 and 210 YadN sub-units.
492 Analysis of the force measurements performed with anti-YadN AFM-probe leads to shorter
493 fimbriae contour lengths. This finding is fully consistent with an unspooling of the probed

View Article Online
DOI: 10.1039/D0NR06840C

494 fimbriae that does not start from their very top end but, instead, from an intermediate position
495 along their main body (**Figure 7**).

496 Three main values are further found for the persistence length of Yad fimbriae unspooled by
497 anti-Yad(C and N) AFM probe (**Figure S7**): 0.4, 0.6 and 1.0 nm. These values are significantly
498 higher (by *ca.* 1 order of magnitude) than those previously reported for bacterial type 1 or type
499 IV fimbriae^{60, 63, 64} and, most importantly, they define persistence lengths that are significantly
500 shorter than a single pilin subunit (7.8 nm, as reported in **Table 4**). Recent AFM and simulation
501 studies demonstrated that a 1 nm value corresponds to a single strand within a fimbria and that
502 lower values of persistence length may be associated to intramolecular deformations and
503 unfolding of pilin subunits.^{45, 65-67} As further reported in previous studies based on AFM
504 measurements, low persistence length values may originate from the stretching of polypeptide
505 segments (as a result of the applied force) and not from the stretching of a polymer chain
506 consisted of globular units.⁶⁸ Accordingly, our results indicate that Yad fimbriae consist of a
507 tubular assembly of easily deformable subunits (*i.e.* with persistence length that is significantly
508 shorter than the subunit size), which fragilize the whole Yad structure when subjected to
509 mechanical stress. This is in line with our observation of broken Yad fimbriae at the substrates
510 surface and of a resulting marked polydispersity in terms of Yad fimbriae length (**Figure 1**).

511 Previous observations of Yad fimbriae using Transmission Electron Microscopy (TEM)
512 suggested that Yad fimbriae could be much more flexible than, for example, type 1 fimbriae.^{30,}
513 ⁴¹ Even though conclusions derived from TEM or cryo-TEM analysis should be considered
514 with caution due to the sample preparation procedures that possibly modify biosurface structure
515 and integrity, this finding is consistent with the absence of successive force plateau regimes in
516 the SMFS force profiles pertaining to Yad, as invoked above. The shorter persistence length of
517 type 1 fimbriae conjugated with the observation of SMFS force plateau regimes for such a
518 structure indicate a larger molecular cohesion and tensile strength as compared to those for Yad

519 structure whose easier unfolding of the composing YadN subunits makes it impossible for the
520 overall Yad structure to maintain cohesion upon withdrawal of the AFM probe, which explains,
521 in turn, the absence of any force plateau in the SMFS profile and the detection of successive
522 abrupt rupture events.

523 The periodicity of the adhesive events along fimbriae backbone, denoted as δL , was evaluated
524 from the distance between two successive adhesive events (**Figure 6** and **Table 2**). For
525 situations where Yad fimbriae are unspooled by anti-YadC and anti-YadN AFM-probes, the
526 large distribution in δL (from few nanometers to 1 μm) is multimodal with four maxima at *ca.*
527 30, 120, 350 and 700 nm. It is found that 40-50% of the probed δL values are in the 0-100 nm
528 range, which indicates that fimbriae unspooling occurs mainly by successive ‘jumps’ of
529 ensembles of 12 YadN subunits. In cases where fimbriae are unspooled by xylosyl AFM-probe,
530 the distribution in δL remains trimodal but, here, the three detected modes are much more
531 clearly defined (77, 243 and 331 nm) with δL values that cover a narrower range (from few
532 nanometers to 500 nm) than that obtained with anti-Yad probes. The well-defined trimodal
533 distribution suggests that unspooling of the Yad fimbriae by Xyl probes takes place upon by
534 successive jump of 10, 31 and 42 YadN subunits. The lesser defined δL distributions measured
535 with the anti YadN and anti YadC probes may originate from the polyclonal nature of the used
536 antibodies that may interact simultaneously with several YadN and YadC subunits, in contrast
537 with xylose that targets only one YadC subunit.

538 Modelling of the SMFS force curves collected with the other galactosyl (Gal, Man and Lac)-
539 grafted AFM-probes shows that the corresponding multimodal distribution of δL (**Figure 6**),
540 with rather ill-defined Gaussian components, basically spread over a large range of values (from
541 few nanometers to 1 μm) with maxima located at larger δL as compared to those identified for
542 Xyl and anti-Yad probes. The dispersion in δL values is somewhat lesser pronounced for
543 mannosyl- and lactosyl-grafted AFM-probes (few nanometers up to 600 nm) than for galactosyl

544 AFM probe. Three maxima of about 200, 350 and 600 nm are found for δL derived from SMFS Manuscript Online
DOI: 10.1039/D0NR06840C

545 force curves measured with galactosyl-grafted AFM-probe, and values of about 130, 230 and

546 400 nm are obtained with the mannosyl-grafted AFM-probe. The interpretation of SMFS

547 experiments performed with the glycosylated AFM-probes is rather complicated, except for the

548 probe grafted with xylosyl specifically recognized by YadC subunit. Instead, galactosyl,

549 lactosyl and mannosyl residues may interact with any of the Yad fimbriae subunits (which

550 includes the YadM, YadK, YadL and YadN components), resulting in unspooling configuration

551 close to that depicted for anti-YadN grafted AFM probe (**Figure 7**). Accordingly, unspooling

552 of the Yad fimbriae by galactosyl-, mannosyl- and lactosyl-grafted AFM-probes possibly occur

553 by successive jumps of sets of 17 up to 104 YadN subunits. It should be further realized that

554 the interpretation of the force curves measured with these functionalities of the AFM probe is

555 all the more difficult as the interactions between glycosylated AFM-probes and Δ_4adh_PcLYad

556 bacterial cell wall may involve macromolecular structures expressed at the cell wall other than

557 the targeted Yad fimbriae. This hypothesis is comforted by the inspection of the adhesion results

558 obtained with Δ_4adh , which features rare adhesive events (but still measurable) between Δ_4adh

559 cell wall and the various substrates adopted in this work (see **Table 3**). Complementary

560 experiments using various cell surface components on mutant strains and surfaces with

561 controlled chemistries other than those tested here could be more relevant to address this issue.

562 We emphasize still the probability of interactions occurrence between galactosyl-, mannosyl-

563 and lactosyl-grafted AFM-probes concerns less than 20% of total force curves, which is 4 to 5

564 times lower than that relevant for the curves obtained with anti-YadN, anti-YadC and xylosyl

565 residue. Here, accordingly, we clearly evidenced that Yad fimbriae interact primarily and

566 strongly with anti-YadN, anti-YadC and xylosylated surfaces whereas interactions in respect

567 with other glycosylated surfaces are significantly lesser frequent and are defined by lower

568 magnitude of the corresponding adhesion forces.

569

View Article Online
DOI: 10.1039/D0NR06840C

570 **On the connection between adhesion properties of Yad fimbriae and Δ_{4adh_PcLyad} cells**
571 **revealed at the molecular and macroscopic scales, respectively.**

572 **Figure 8** reports the concentrations of Δ_{4adh_PcLyad} bacteria adhered at the surface of SAM-
573 Xyl, SAM-anti YadC and SAM-anti YadN (**Figure 2**) as a function of the median adhesion
574 forces measured by SMFS at the molecular scale between Yad fimbriae and Xyl-, anti YadC-
575 and anti YadN-AFM probes, respectively (**Figure 4**). The data obtained for the other
576 glycosylated surfaces and glycosyl-decorated AFM probes further complete the comparison
577 between Yad fimbriae adhesion features assessed at the molecular scale and the macroscopic
578 Δ_{4adh_PcLyad} cells adhesion properties evaluated from standard fluorescence-based counting
579 method. The dispersion of the points in the x -axis of **Figure 8** reflects the range of maximal
580 adhesion forces measured over the various multimodal distribution's maxima pictured in
581 **Figure 4**.

582 **Figure 8** evidences the existence of an exponential-like dependence for the surface
583 concentration of adhered cells on the corresponding adhesion force measured at the relevant
584 molecular scale. For the sake of quantitative illustration, 100 pN interaction force between a
585 single bacterium cell wall (as selected for the SMFS experiments) and substrate surface leads
586 to the adhesion of about 10^6 cells cm^{-2} , and 200 pN leads to the adhesion of about 10^8 cells cm^{-2} .
587 The latter surface concentration corresponds to a fully covered surface if assuming that all
588 adhered bacteria adopt a lying cylindrical configuration at the substrate surface. To the best of
589 our knowledge, the influence of substrate surface chemistry on bacterial adhesion has been
590 rarely addressed both at the macroscopic and molecular scales^{69, 70} and the experimental results
591 detailed in this work highlight the intimate connection between the nanoscale adhesion features
592 of the Yad fimbriae and the resulting bacterial adhesion behavior. They therefore support
593 numerous theoretical studies about the dependence of bacterial adhesion on surface chemistry⁷¹⁻

594 ⁷⁴ left, so far, without solid experiments-based evidence of the relationship between adhesion
595 properties detailed at the various scales of interest, from the molecular adhesion event to the
596 cell adsorption process. The exponential relationship revealed by **Figure 8** further suggests the
597 applicability of an effective Boltzmann-like dependence for the surface concentration of
598 adhered bacteria on the operational molecular adhesion force F_{adh} , recalling that F_{adh} may be
599 formally converted into an adhesion energy per unit surface area upon dividing F_{adh} by a
600 characteristic length scale, this ratio having the dimension of a superficial tension. Last, the
601 results obtained in this work support that assessment of bacterial adhesion features can not be
602 reduced to the standard DLVO-inspired strategy that consists in measuring surface charge of
603 the bacteria (with all ‘‘ins and outs’’ related to this issue, see e.g. the demonstration by Duval
604 and coworkers that the zeta-potential concept is physically irrelevant for bacteria,⁵⁶ and
605 references therein⁵⁹ and surface charge of the deposition substrate. Previous work on
606 aggregation of bacteria decorated or not by self-associating Ag43 adhesins demonstrated that
607 reasoning on the basis of the (similar) pH-dependent macroscopic surface charge of bacteria
608 (evaluated by electrophoresis) decorated or not by Ag43 could not explain the differentiated
609 auto-aggregation properties of these cells.⁷⁵ Instead a detailed SFMS-based analysis could
610 clarify the molecular origin of the observed aggregation features of bacteria devoid or not of
611 Ag43. In addition, the salinity conditions operational in our SMFS measurements (with overall
612 ionic strength well above 100 mM) are such that the surface charge of the bacteria are
613 significantly screened, meaning that short range coulombic forces, dipole-dipole interactions
614 and, obviously, specific interaction forces are here the relevant determinants of Yad fimbriae
615 binding to the selected substrates. In line with these results, our results clearly evidence a strong
616 connection between the adhesion forces measured at the molecular scale (not accounted for in
617 standard DLVO theory) and the macroscopic adhesion properties of Yad-decorated bacteria.
618

619 **Conclusion**

View Article Online
DOI: 10.1039/D0NR06840C

620 The adhesion of Yad fimbriae on model substrates defined by different and controlled surface
621 chemistries are here evaluated at the molecular scale by Single Molecule Force Spectroscopy.
622 The results evidence that the affinity of Yad fimbriae for xylose is as strong as that for
623 polyclonal anti-YadC and anti-YadN antibodies (*ca.* 80 to 300 pN). In contrast, the adhesion
624 features of Yad fimbriae on -NH₂, -OH, -COOH, -CH₃, Lactose, Mannose and Galactose
625 terminated self-assembled monolayers indicate non specificity of the interactions of Yad with
626 these surfaces. A clear connection between these findings, relevant at the molecular scale, and
627 the adhesion properties of *E. coli* decorated or not by Yad fimbriae is further established. This
628 nano-macro relationship pinpoints the importance of the study of nanoscale specific interactions
629 of fimbriae with their cognate ligands. Such a study opens the way to the design of efficient
630 anti-adhesive molecules that could be used in anti-virulence strategies against pathogenic
631 bacteria.

633 **Acknowledgments**

634 The authors thank the Spectroscopy and Microscopy Service Facility (SMI) of LCPME
635 (Université de Lorraine-CNRS – <http://www.lcpme.cnrs-nancy.fr>) where most of experiments
636 were performed. GF and JFLD further thank C. Caillet of the LIEC for preliminary assessment
637 of the fragility of parietal structures decorating Δ_{4adh} and Δ_{4adh_PcLyad} cells. We thank F.
638 Larsonneur for Δ_{4adh_PcLyad} strain construction. Work in the group of CB was supported by
639 an Institut Pasteur grant, by the French government's Investissement d'Avenir Program,
640 Laboratoire d'Excellence "Integrative Biology of Emerging Infectious Diseases" (grant
641 n°ANR-10-LABX-62-IBEID) and the *Fondation pour la Recherche Médicale* (grant no.
642 DEQ20180339185). YC was supported by a MENESR (Ministère Français de l'Education
643 Nationale, de l'Enseignement Supérieur et de la Recherche) fellowship.

644

645

646 **Supporting Information**

647 Supplementary AFM images of Δ_4adh and Δ_4adh_PcLyad cells (**Figure S1**), IRRAS spectra of
648 the various model SAM substrates selected in this study (**Figure S2**), Representative
649 epifluorescence images of Δ_4adh_PcLyad on the different SAM substrates tested (**Figure S3**),
650 Representative epifluorescence images of Δ_4adh on the different SAM substrates tested (**Figure**
651 **S4**), Illustrative SMFS force measurements for Δ_4adh cell wall interacting with AFM probes
652 featuring YadC, YadN, xylose, galactose, mannose and lactose functionalities (**Figure S5**),
653 Statistic distribution of the number of adhesive events per retraction force curve recorded for
654 Δ_4adh_PcLyad cell wall in interaction with AFM probes featuring YadC, YadN, xylose,
655 galactose, mannose and lactose functionalities (**Figure S6**), As in **Figure S6**, *albeit* for the
656 persistence length of Yad fimbriae (**Figure S7**).

657 **References:**View Article Online
DOI: 10.1039/D0NR06840C

- 658 1. D. M. Costa, K. Johani, D. S. Melo, L. K. O. Lopes, L. K. O. Lopes Lima, A. F. V.
659 Tipple, H. Hu and K. Vickery, *Lett. Appl. Microbiol.*, 2019, **68**, 269-276.
- 660 2. S. Galié, C. García-Gutiérrez, E. M. Miguélez, C. J. Villar and F. Lombó, *Frontiers in*
661 *microbiology*, 2018, **9**, 898-898.
- 662 3. D. Lebeaux, J.-M. Ghigo and C. Beloin, *Microbiol. Mol. Biol. Rev.*, 2014, **78**, 510-543.
- 663 4. J. Luis Del Pozo, *Expert Review of Anti-Infective Therapy*, 2018, **16**, 51-65.
- 664 5. A. Alvarez-Ordóñez, L. M. Coughlan, R. Briandet and P. D. Cotter, in *Annual Review*
665 *of Food Science and Technology, Vol 10*, eds. M. P. Doyle and D. J. McClements, 2019,
666 vol. 10, pp. 173-195.
- 667 6. J. W. Leff and N. Fierer, *PLoS One*, 2013, **8**, e59310.
- 668 7. J. J. Luna-Guevara, M. M. P. Arenas-Hernandez, C. Martínez de la Peña, J. L. Silva and
669 M. L. Luna-Guevara, *International Journal of Microbiology*, 2019, **2019**, 2894328.
- 670 8. C. Berger, S. Sodha, R. Shaw, P. Griffin, D. Pink, P. Hand and G. Frankel,
671 *Environmental microbiology*, 2010, **12**, 2385-2397.
- 672 9. G. Ávila-Quezada, E. Sánchez, A. A. Gardea-Béjar and E. Acedo-Félix, *New Zealand*
673 *Journal of Crop and Horticultural Science*, 2010, **38**, 47-55.
- 674 10. S. Kampmeier, M. Berger, A. Mellmann, H. Karch and P. Berger, *Curr Top Microbiol*
675 *Immunol*, 2018, **416**, 117-148.
- 676 11. J. P. Cramer, in *Emerging Infectious Diseases*, eds. Ö. Ergönül, F. Can, L. Madoff and
677 M. Akova, Academic Press, Amsterdam, 2014, DOI: [https://doi.org/10.1016/B978-0-](https://doi.org/10.1016/B978-0-12-416975-3.00017-0)
678 [12-416975-3.00017-0](https://doi.org/10.1016/B978-0-12-416975-3.00017-0), pp. 213-227.
- 679 12. E. Köckerling, L. Karrasch, A. Schweitzer, O. Razum and G. Krause, *Frontiers in*
680 *Public Health*, 2017, **5**.
- 681 13. A. Caprioli, G. Scavia and S. Morabito, *Microbiology spectrum*, 2014, **2**.
- 682 14. J. B. Kaper and A. D. O'Brien, *Microbiology spectrum*, 2014, **2**.
- 683 15. E. J. Boll, J. Ayala-Lujan, R. L. Szabady, C. Louissaint, R. Z. Smith, K. A. Krogfelt, J.
684 P. Nataro, F. Ruiz-Perez and B. A. McCormick, *mBio*, 2017, **8**, e00717-00717.
- 685 16. M. A. Rendon, Z. Saldana, A. L. Erdem, V. Monteiro-Neto, A. Vazquez, J. B. Kaper, J.
686 L. Puente and J. A. Giron, *Proc. Natl. Acad. Sci. USA*, 2007, **104**, 10637-10642.
- 687 17. C. Lang, A. Fruth, G. Holland, M. Laue, S. Mühlen, P. Dersch and A. Flieger, *Emerging*
688 *Microbes & Infections*, 2018, **7**, 1-16.
- 689 18. S. Knutton, R. Shaw, M. K. Bhan and A. S. McNeish, *Pediatr. Res.*, 1990, **27**, 530-530.

- 690 19. C. Moreira, S. Carneiro, J. Nataro, L. Trabulsi and W. Elias, *FEMS Microbiol. Lett.* View Article Online
DOI: 10.1039/D0NR06840C 2003, **226**, 79-85.
691
- 692 20. P. Luthje and A. Brauner, in *Advances in Microbial Physiology, Vol 65: Advances in*
693 *Bacterial Pathogen Biology*, ed. R. K. Poole, 2014, vol. 65, pp. 337-372.
- 694 21. P. Klemm, V. Hancock and M. A. Schembri, *Environ. Microbiol. Rep.*, 2010, **2**, 628-
695 640.
- 696 22. V. Ageorges, R. Monteiro, S. Leroy, C. M. Burgess, M. Pizza, F. Chaucheyras-durand
697 and M. Desvaux, *FEMS Microbiol. Rev.*, 2020, **44**, 314-350.
- 698 23. A. Monserrat-Martinez, Y. Gambin and E. Sierrecki, *Int. J. Mol. Sci.*, 2019, **20**, 1255.
- 699 24. J. J. Psonis and D. G. Thanassi, *EcoSal Plus*, 2019, **8**.
- 700 25. S. Geibel and G. Waksman, *Biochim. Biophys. Acta-Mol. Cell Res.*, 2014, **1843**, 1559-
701 1567.
- 702 26. C. G. Korea, J. M. Ghigo and C. Beloin, *BioEssays*, 2011, **33**, 300-311.
- 703 27. D. J. Wurpel, S. A. Beatson, M. Totsika, N. K. Petty and M. A. Schembri, *PLoS One*,
704 2013, **8**.
- 705 28. F. Dziva, H. Hauser, T. R. Connor, P. M. van Diemen, G. Prescott, G. C. Langridge, S.
706 Eckert, R. R. Chaudhuri, C. Ewers, M. Mellata, S. Mukhopadhyay, R. Curtiss, III, G.
707 Dougan, L. H. Wieler, N. R. Thomson, D. J. Pickard and M. P. Stevens, *Infect. Immun.*,
708 2013, **81**, 838-849.
- 709 29. R. Verma, T. C. Galvao Rojas, R. P. Maluta, J. L. Leite, L. P. Mendes da Silva, G.
710 Nakazato and W. D. da Silveira, *Infect. Immun.*, 2016, **84**, 187-193.
- 711 30. F. Larssonneur, F. Martín, A. Mallet, M. Martinez-gil, V. Semetey, J. M. Ghigo and C.
712 Beloin, *Environmental Microbiology*, 2016, **18**, 5228-5248.
- 713 31. K. C. Gross and C. E. Sams, *Phytochemistry*, 1984, **23**, 2457-2461.
- 714 32. A. P. S. Sandhu, G. S. Randhawa and K. S. Dhugga, *Molecular Plant*, 2009, **2**, 840-
715 850.
- 716 33. E. M. S. M. Gaspar, I. S. Nunes and J. F. Lopes, *Xylose: Production, Consumption and*
717 *Health Benefits*, 2012, 43-67.
- 718 34. C. F. Carson and T. V. Riley, *Communicable diseases intelligence quarterly report*,
719 2003, **27 Suppl**, S143-146.
- 720 35. I. Ofek, D. L. Hasty and N. Sharon, *FEMS Immunol. Med. Microbiol.*, 2003, **38**, 181-
721 191.
- 722 36. A. Asadi, S. Razavi, M. Talebi and M. Gholami, *Infection*, 2019, **47**, 13-23.

- 723 37. C. K. Cusumano, J. S. Pinkner, Z. Han, S. E. Greene, B. A. Ford, J. R. Crowley, J. P. Henderson, J. W. Janetka and S. J. Hultgren, *Science Translational Medicine*, 2011, **3**,
724 109ra115-109ra115. View Article Online
DOI: 10.1039/D0NR06840C
- 726 38. J. Ohlsson, J. Jass, B. E. Uhlin, J. Kihlberg and U. J. Nilsson, *ChemBioChem*, 2002, **3**,
727 772-779.
- 728 39. M.-C. Duvernoy, T. Mora, M. Ardre, V. Croquette, D. Bensimon, C. Quilliet, J.-M. Ghigo, M. Balland, C. Beloin, S. Lecuyer and N. Desprat, *Nature Communications*,
729 2018, **9**, 1-10.
730
- 731 40. P. P. Cherepanov and W. Wackernagel, *Gene*, 1995, **158**, 9-14.
- 732 41. C. G. Korea, R. Badouraly, M. C. Prevost, J. M. Ghigo and C. Beloin, *Environ
733 Microbiol*, 2010, **12**, 1957-1977.
- 734 42. L. Wildling, B. Unterauer, R. Zhu, A. Rupprecht, T. Haselgrubler, C. Rankl, A. Ebner,
735 D. Vater, P. Pollheimer, E. E. Pohl, P. Hinterdorfer and H. J. Gruber, *Bioconjug Chem*,
736 2011, **22**, 1239-1248.
- 737 43. A. Ebner, L. Wildling, R. Zhu, C. Rankl, T. Haselgrubler, P. Hinterdorfer and H. J. Gruber, in *Stm and Afm Studies On*, Springer-Verlag Berlin, Berlin, 2008, vol. 285, pp.
738 29-76.
739
- 740 44. A. Ebner, L. Wildling, A. S. Kamruzzahan, C. Rankl, J. Wruss, C. D. Hahn, M. Holzl,
741 R. Zhu, F. Kienberger, D. Blaas, P. Hinterdorfer and H. J. Gruber, *Bioconjug Chem*,
742 2007, **18**, 1176-1184.
- 743 45. A. Jacquot, C. Sakamoto, A. Razafitianamaharavo, C. Caillet, J. Merlin, A. Fahs, J. M. Ghigo, C. Beloin, J. F. L. Duval and G. Francius, *J. Biomed. Nanotechnol.*, 2014, **10**,
744 3361-3372.
745
- 746 46. A. Ebner, P. Hinterdorfer and H. J. Gruber, *Ultramicroscopy*, 2007, **107**, 922-927.
- 747 47. H. Schillers, I. Medalsy, S. Hu, A. L. Slade and J. E. Shaw, *J. Mol. Recognit.*, 2016, **29**,
748 95-101.
- 749 48. K. Xu, W. Sun, Y. Shao, F. Wei, X. Zhang, W. Wang and P. Li, *Nanotechnology
750 Reviews*, 2018, **7**, 605-621.
- 751 49. P. Polyakov, C. Soussen, J. Duan, J. F. L. Duval, D. Brie and G. Francius, *PLoS One*,
752 2011, **6**, e18887.
- 753 50. A. Janshoff, M. Neitzert, Y. Oberdorfer and H. Fuchs, *Angew Chem Int Ed Engl*, 2000,
754 **39**, 3212-3237.
- 755 51. C. Ortiz and G. Hadziioannou, *Macromolecules*, 1999, **32**, 780-787.
- 756 52. E. Wiercigroch, E. Szafraniec, K. Czamara, M. Z. Pacia, K. Majzner, K. Kochan, A. Kaczor, M. Baranska and K. Malek, *Spectrochimica acta. Part A, Molecular and
757 biomolecular spectroscopy*, 2017, **185**, 317-335.
758

- 759 53. H. A. Wells and R. H. Atalla, *J. Mol. Struct.*, 1990, **224**, 385-424.
- 760 54. R. Zimmermann, J. F. L. Duval and C. Werner, *Curr. Opin. Colloid Interface Sci.*, 2019,
761 **44**, 177-187.
- 762 55. J. Song, J. F. L. Duval, M. A. Stuart, H. Hillborg, U. Gunst, H. F. Arlinghaus and G. J.
763 Vancso, *Langmuir*, 2007, **23**, 5430-5438.
- 764 56. J. F. L. Duval and F. Gaboriaud, *Curr. Opin. Colloid Interface Sci.*, 2010, **15**, 184-195.
- 765 57. F. Gaboriaud, M. L. Gee, R. Strugnell and J. F. L. Duval, *Langmuir*, 2008, **24**, 10988-
766 10995.
- 767 58. M. Castelain, S. Ehlers, J. Klinth, S. Lindberg, M. Andersson, B. E. Uhlin and O. Axner,
768 *European biophysics journal : EBJ*, 2011, **40**, 305-316.
- 769 59. F.-J. Chen, C.-H. Chan, Y.-J. Huang, K.-L. Liu, H.-L. Peng, H.-Y. Chang, G.-G. Liou,
770 T.-R. Yew, C.-H. Liu, K. Hsu and L. Hsu, *J. Bacteriol.*, 2011, **193**, 1718-1725.
- 771 60. M. Andersson, O. Björnham, M. Svantesson, A. Badahdah, B. E. Uhlin and E. Bullitt,
772 *J. Mol. Biol.*, 2012, **415**, 918-928.
- 773 61. M. Forero, O. Yakovenko, E. V. Sokurenko, W. E. Thomas and V. Vogel, *PLoS Biol.*,
774 2006, **4**, e298.
- 775 62. L. A. Pratt and R. Kolter, *Mol. Microbiol.*, 1998, **30**, 285-293.
- 776 63. P. M. Silverman and M. B. Clarke, *Integrative Biology*, 2010, **2**, 25-31.
- 777 64. Hendrick W. de Haan, *Biophys. J.*, 2016, **111**, 2263-2273.
- 778 65. J. Rheinlaender, A. Gräbner, L. Ott, A. Burkovski and T. E. Schäffer, *European
779 biophysics journal : EBJ*, 2012, **41**, 561-570.
- 780 66. M. Castelain, M.-P. Duviau, A. Canette, P. Schmitz, P. Loubière, M. Cocaign-Bousquet,
781 J.-C. Piard and M. Mercier-Bonin, *PLoS One*, 2016, **11**, e0152053-e0152053.
- 782 67. W. Pönisch, C. A. Weber, G. Juckeland, N. Biais and V. Zaburdaev, *New Journal of
783 Physics*, 2017, **19**, 015003.
- 784 68. , !!! INVALID CITATION !!! 57, 59, 60.
- 785 69. F. Alam, S. Kumar and K. M. Varadarajan, *ACS Biomater. Sci. Eng.*, 2019, **5**, 2093-
786 2110.
- 787 70. R. Bos, H. C. van der Mei and H. J. Busscher, *FEMS Microbiol. Rev.*, 1999, **23**, 179-
788 230.
- 789 71. F. Pan, S. Altenried, M. Liu, D. Hegemann, E. Bülbül, J. Moeller, W. W. Schmahl, K.
790 Maniura-Weber and Q. Ren, *Materials Horizons*, 2020, **7**, 93-103.

View Article Online
DOI: 10.1039/D0NR06840C

- 791 72. J. K. Oh, Y. Yegin, F. Yang, M. Zhang, J. Li, S. Huang, S. V. Verkhoturov, E. A. Schweikert, K. Perez-Lewis, E. A. Scholar, T. M. Taylor, A. Castillo, L. Cisneros-Zevallos, Y. Min and M. Akbulut, *Sci Rep*, 2018, **8**, 17247. New Article Online
DOI: 10.1039/D0NR06840C
- 794 73. A. O. Eskhan and N. I. Abu-Lail, *Colloid Polym. Sci.*, 2014, **292**, 343-353.
- 795 74. H. J. Busscher, W. Norde and H. C. van der Mei, *Appl. Environ. Microbiol.*, 2008, **74**,
796 2559-2564.
- 797 75. A. Jacquot, C. Sakamoto, A. Razafitianamarahavo, C. Caillet, J. Merlin, A. Fahs, J. M.
798 Ghigo, J. F. L. Duval, C. Beloin and G. Francius, *Nanoscale*, 2014, **6**, 12665-12681.
- 799 76. G. Yachdav, E. Kloppmann, L. Kajan, M. Hecht, T. Goldberg, T. Hamp, P.
800 Hönigschmid, A. Schafferhans, M. Roos, M. Bernhofer, L. Richter, H. Ashkenazy, M.
801 Punta, A. Schlessinger, Y. Bromberg, R. Schneider, G. Vriend, C. Sander, N. Ben-Tal
802 and B. Rost, *Nucleic Acids Res.*, 2014, **42**, W337-W343.
- 803

804

Tables

View Article Online
DOI: 10.1039/D0NR06840C

805

806 **Table 1.** Details on the genetic profiles of Δ_4adh and Δ_4adh_PcLyad strains and on their
807 constructions.

Strain or plasmid	Relevant genotypic and phenotypic characteristics	Source or reference
Δ_4adh	MG1655_ <i>gfp_ΔfliE- R::cat_Δflu::FRT_ΔfimAICDFGH::zeo_ΔcsgA::aadA7</i> GFP+, no flagella, no type 1 fimbriae, no Ag43, no curli, Amp ^R , Cm ^R , Zeo ^R , Spec ^R	39
PcLyad	MG1655_ <i>kmPcLyad</i> , <i>yad</i> operon under the control of the constitutive lambda P _R promoter, Km ^R	41
Δ_4adh_PcLyad	MG1655_ <i>gfp_ΔfliE- R::cat_Δflu::FRT_ΔfimAICDFGH::zeo_ΔcsgA::aadA7_</i> <i>kmPcLyad</i> , Km ^R P1vir transduction of <i>kmPcLyad</i> from strain PcLyad into <u>Δ_4adh</u> GFP+, no flagella, no type 1 fimbriae, no Ag43, no curli, constitutive expression of the <i>yad</i> operon, Amp ^R , Cm ^R , Zeo ^R , Spec ^R , Km ^R	This work

809

810

811

813 **Table 2.** Physico-chemical parameters derived from Single Molecule Force Spectroscopy (SMFS) measurements performed on Δ_{4adh_PcLyad}
 814 bacteria using different functionalities of the AFM probe (indicated). **The evaluation of the parameters is performed by modeling the measured
 815 force-curves using eq 1, and given values correspond to maxima of the corresponding multimodal distributions and their standard deviations. * The
 816 values reported in this column refer to the % of the force curves featuring at least one adhesive event. See text for further details.

AFM-Probes (# curves)	Adhesive events (%)*	Adhesion forces (nN)**	Maximal extension (nm)**	Persistence length (nm)**	Peak-to-peak distance (nm)
Anti-YadC (6487)	98.0 ± 1.1	0.081 ± 0.061	936 ± 170	0.45 ± 0.12	37 ± 40
		0.148 ± 0.079	1234 ± 205	0.60 ± 0.29	118 ± 112
		0.245 ± 0.084	1648 ± 77	1.05 ± 0.78	366 ± 178
Anti-YadN (8210)	92.5 ± 3.5	0.078 ± 0.045	247 ± 102	0.38 ± 0.20	709 ± 255
		0.157 ± 0.078	761 ± 233	0.67 ± 0.32	23 ± 54
		0.302 ± 0.081		1.31 ± 1.07	122 ± 107
Xyl (6715)	87.3 ± 5.7	0.097 ± 0.066	371 ± 66	0.35 ± 0.23	77 ± 49
		0.180 ± 0.072	605 ± 85		243 ± 53
		0.339 ± 0.121	827 ± 72		331 ± 48
Gal (4772)	19.1 ± 4.2	0.058 ± 0.054	1006 ± 68	0.29 ± 0.16	191 ± 90
		0.177 ± 0.104	1194 ± 59		355 ± 185
			673 ± 162		0.62 ± 0.35
Lac (6062)	22.7 ± 6.8	0.064 ± 0.072	589 ± 106	0.98 ± 0.65	131 ± 104
		0.159 ± 0.091	792 ± 98		235 ± 83
			953 ± 89		403 ± 222
			1178 ± 182		
			1407 ± 208		

Man (5258)	15.3 ± 3.9	0.076 ± 0.081 0.183 ± 0.078	241 ± 132 435 ± 106 576 ± 97	0.35 ± 0.11 0.58 ± 0.25 0.95 ± 0.67	216 ± 94 285 ± 83 411 ± 184 815 ± 71
---------------	------------	--------------------------------	------------------------------------	---	---

817

818

819

820

Table 3. As in Table 2 *albeit* for Δ_4adh cells. ‘nd’: ‘not determined.

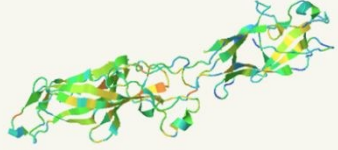
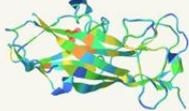
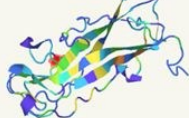
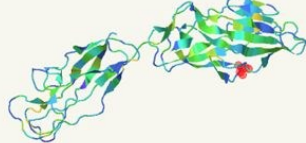
AFM-Probes (# curves)	Adhesive events (%)*	Adhesion forces (nN)**	Maximal extension (nm)**	Persistence length (nm)**	Peak-to-peak distance (nm)
Anti-YadC (2772)	0.7 ± 0.9	nd	nd	nd	nd
Anti-YadN (3894)	2.1 ± 1.7	nd	nd	nd	nd
Xyl (2721)	1.3 ± 1.5	nd	nd	nd	nd
Gal (2772)	4.9 ± 2.2	nd	nd	nd	nd
Lac (3267)	2.7 ± 0.8	nd	nd	nd	nd
Man (3662)	5.0 ± 3.3	nd	nd	nd	nd

821

822

823

824 **Table 4.** Amino acids sequences, characteristics and most probable structures of YadC and YadN sub-unit of Yad fimbriae determined using
 825 PredictProtein, an online open resource for prediction of protein structural and functional features according to integrated methods.⁷⁶

Peptide	Amino acid sequence	Structure	Characteristics
YadC	MKTIFRYILF LALYSCCNTV SAYTSFIVGN NAGVDNYRGP STAAQMTFNY TSTASNLVfy KPTQLGPTGV KMYWSYLDTG TGGGILYCNT SGRANPGPIT IENAMVYSGK DYGGHKLfnt SVPGLYYTML ISRVWSAYDT ITDIQSPGIY IGDPSNQEFF FSVTDSLQQT KGCNKADDDYD KFWAIGGIVH NITVEFYTDT NFDPTLNQQV QLSSSSNYLY SFKAYSPGTK VVDHSNHIYV NFTLNNVKLT LPTCFTSILT GPSVNGSTVR MGEYSSGTIK NGASPVPFDI SLQNCIRVRN IETKLVTKV GTQNTQLLGN TLTGSTAAKG VGVLIELAT SKNPLMTLKP NDTNSVYIDY ETEDDTSdgv YPNQNGTSQ PLHFQATLKQ DGNIAIEPGE FKATSTFQVT YP		Amino acids : 412 Total charge : 0 Mw : 52253 g/mol Length : 13.1 nm
YadN	MSKKLGFALS GLMLAMVAGT ASADMDGGQL NISGLVVDNT CETRVDGGNK DGLILLQTAT VGEIDAGVLN DTVGAKAKPF SITVDCSKAN PNPSTAKMT FGSVFFGNSK GTLNNDMSIN NPSDGVNIAL HNIDGSTIKQ VQINNPdvy TKALDATTKS AVYDFKASYV RAVADQTATA GYVKTNTAYT ITYQ		Amino acids : 194 Total charge : - 1 Mw : 23573 g/mol Length : 7.8 nm
FimA	MKIKTLAIVV LSALSLSSTA ALAAATTvng GTVHFkgevV NAACAVDAGS VDQTVQLGQV RTASLAQEGA TSSAVGFNIQ LNDCDTNVAS KAAVAFLGTA IDAGHTNVLA LQSSAAGSAT NVGVQILDRT GAALTLDGAT FSSETTLNNG TNTIPFQARY FATGAATPGA ANADATFKVQ YQ		Amino acids : 182 Total charge : - 1 Mw : 21356 g/mol Length : 7.2 nm
FimH	MKRvITLFAV LLMGWSVNAW SFACKTANGT AIPIGGGSAN VYVNLAPVVN VGQNLVVDLS TQIFCHNDYP ETITDYVTLQ RGSAYGGVLS NFSGTVKYSG SSYPFPTTSE TPRVVYNSRT DKPWPVALYL TPVSSAGGVA IKAGSLIAVL ILRQTNnyNS DDFQFVwniy ANNDVVVPTG GCDVSARDVT VTLPDYPGSV PIPLTVYCAK SQNLGYYLSG TTADAGNSIF TNTASFPAQ GVGVLTRNG TIIPANNTVS LGAVGTSAVS LGLTANYART GGQVTAGNVQ SIIGVTFVYQ		Amino acids : 300 Total charge : +2 Mw : 36829 g/mol Length : 12.3 nm

827 **Figure captions**

828

829 **Figure 1.** Images of *E. coli* Δ_{4adh} _PcLyad cells and Yad fimbriae recorded by AFM operated
830 in PeakForce Tapping mode under air conditions at 23°C (scan rate: 0.95 Hz, samples/line: 512,
831 Peak Force setpoint: 0.876 nN, Peak Force amplitude: 120 nm, PFT Gain: 6). (a), (b) a single
832 bacterium; (c), (d) identification of several Yad fimbriae with their corresponding height profile
833 (e) and (f), respectively. The white squares in (b) define the zoom regions given in (c) and (d).

834

835 **Figure 2.** Adhesion (a) and surface coverage (b) of *E. coli* Δ_{4adh} and Δ_{4adh} _PcLyad cells after
836 2 hours incubation onto several SAMs-coated gold substrates covered by YadC, YadN
837 antibodies, xylose (Xyl), galactose (Gal), lactose (Lac), mannose (Man), or with -OH, -CH₃, -
838 NH₂ and -COOH terminated alkanethiols. ANOVA test was used to compare the differences
839 in the median adhesion values for *E. coli* Δ_{4adh} and Δ_{4adh} _PcLyad; there is a statistically
840 significant difference for * p value < 0.050 (no difference for p value > 0.1).

841

842 **Figure 3.** Illustrative force vs. separation distance profiles (black circles) measured by SMFS
843 upon withdrawal of several AFM-probes (functionalized with anti-YadC, anti-YadN
844 antibodies, xylose (Xyl), galactose (Gal), lactose (Lac) and mannose (Man)) from cell wall of
845 *E. coli* Δ_{4adh} _PcLyad. Red lines correspond to theoretical fitting on the basis of the Worm-
846 Like-Chain model (eq 1).

847

848 **Figure 4.** Statistic distribution of the adhesion forces between *E. coli* Δ_{4adh} _PcLyad cells and
849 the different AFM-probes functionalized with anti-YadC, anti-YadN antibodies, xylose (Xyl),
850 galactose (Gal), lactose (Lac) and mannose (Man) (indicated). Red lines correspond to
851 decomposition of the distribution into fundamental Gaussian components.

852

View Article Online
DOI: 10.1039/D0NR06840C

853 **Figure 5.** Statistic distribution of the maximal rupture distances (or maximal Yad fimbriae
854 elongation prior to rupture) estimated from the SMFS force-distance curves measured for *E.*
855 *coli* Δ_{4adh_PcLyad} cells interacting with AFM-probes functionalized with anti-YadC, anti-
856 YadN antibodies, xylose (Xyl), galactose (Gal), lactose (Lac) and mannose (Man) (indicated).
857 Red lines correspond to decomposition of the distribution into fundamental Gaussian
858 components.

859

860 **Figure 6.** Statistic distribution of the distance between two successive adhesive events detected
861 on the SMFS force-curves collected for *E. coli* Δ_{4adh_PcLyad} cells in interaction with AFM-
862 probes functionalized with anti-YadC, anti-YadN antibodies, xylose (Xyl), galactose (Gal),
863 lactose (Lac) and mannose (Man) (indicated).

864

865 **Figure 7.** Schematics for the structure of Yad fimbriae and its possible conformation during
866 stretching by antibodies or xylose residues grafted at the apex of AFM probes.

867

868 **Figure 8.** Dependence of the surface concentration of bacteria adhered onto SAMs-coated gold
869 substrates covered by anti-YadC, anti-YadN antibodies, xylose (Xyl), galactose (Gal), lactose
870 (Lac), mannose (Man) on their corresponding median adhesive interactions measured between
871 AFM-probes functionalized with anti-YadC, anti-YadN antibodies, xylose (Xyl), galactose
872 (Gal), lactose (Lac) and mannose (Man) (specified in the figure) and individual *E. coli*
873 Δ_{4adh_PcLyad} cells. Dashed line corresponds to linear fitting of the data in semi-logarithmic
874 scale.

875

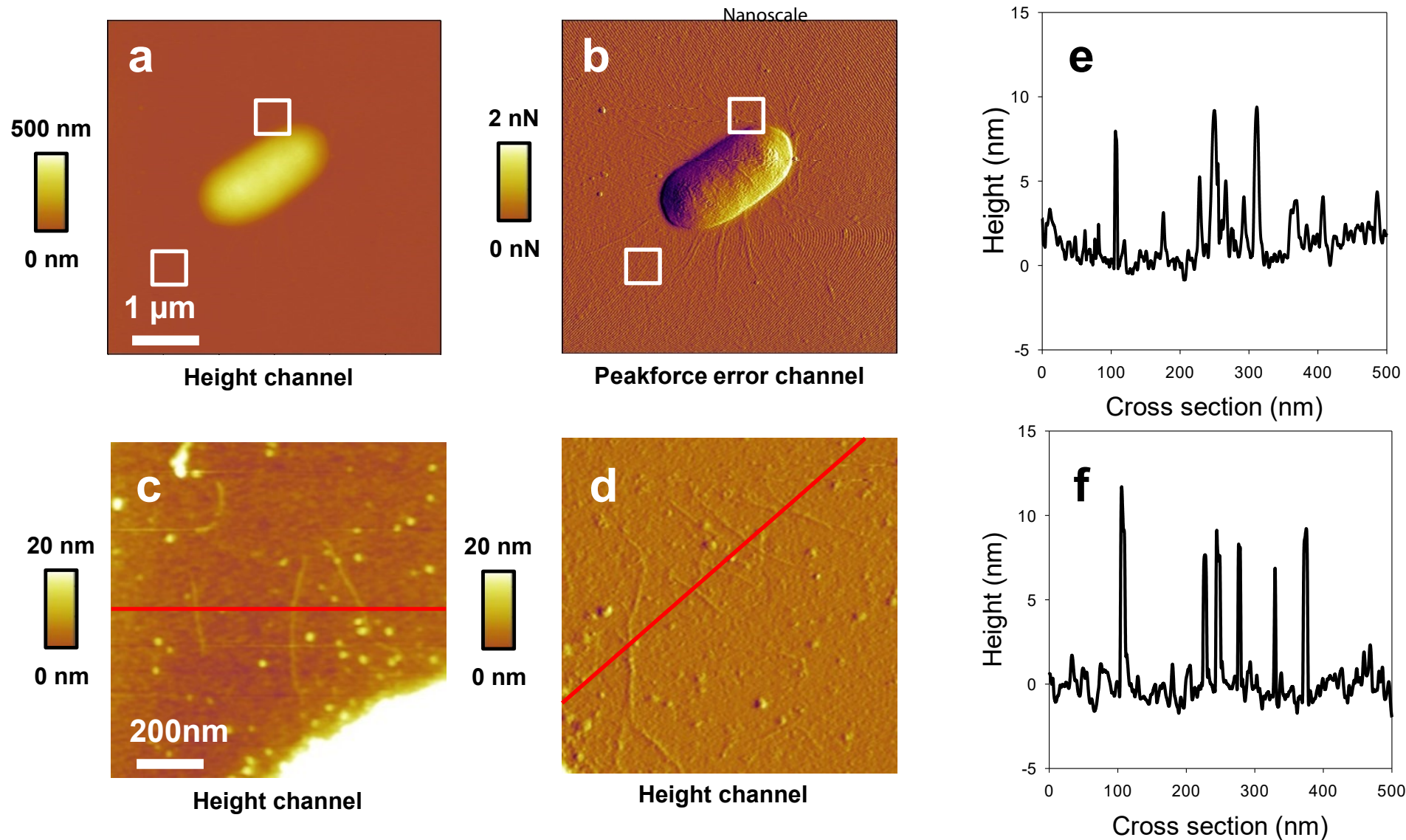


Figure 1 : Figure 1. Images of *E. coli* $\Delta 4adh_PcLyad$ cells and Yad fimbriae recorded by AFM operated in PeakForce Tapping mode under air conditions at 23°C (scan rate: 0.95 Hz, samples/line: 512, Peak Force setpoint: 0.876 nN, Peak Force amplitude: 120 nm, PFT Gain: 6). (a), (b) a single bacterium; (c), (d) identification of several Yad fimbriae with their corresponding height profile (e) and (f), respectively. The white squares in (b) define the zoom regions given in (c) and (d).

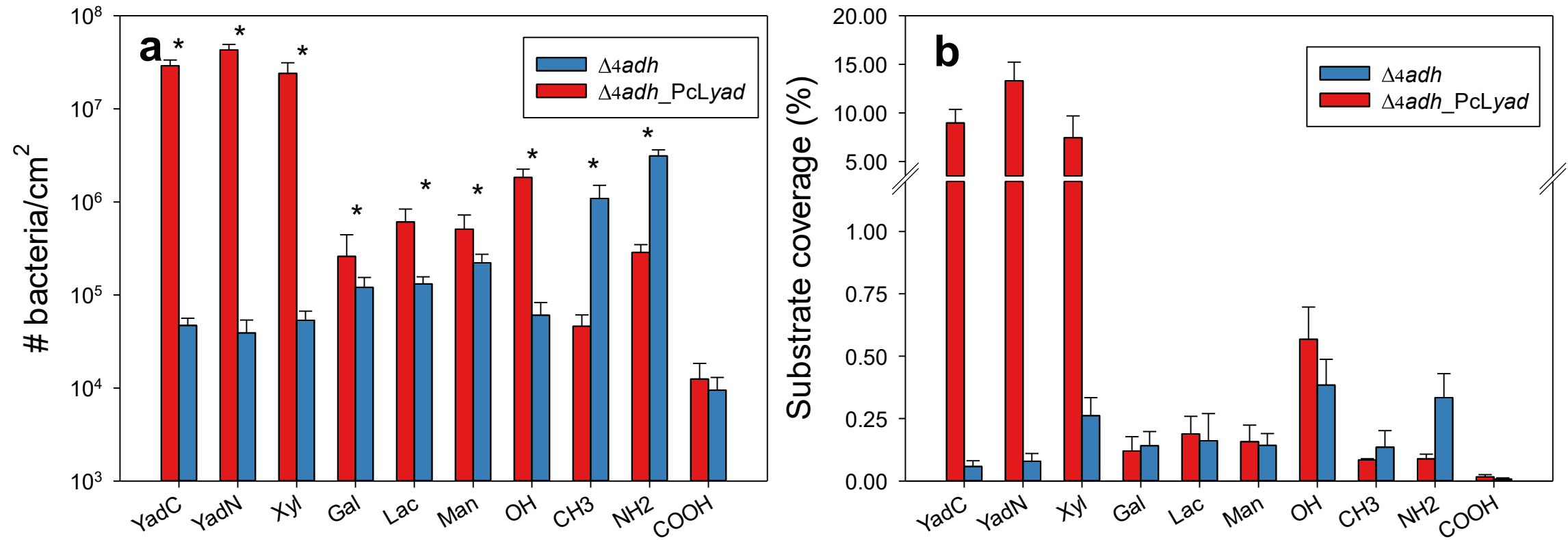


Figure 2 : Adhesion (a) and surface coverage (b) of *E. coli* Δ_4adh_PcLyad and Δ_4adh after 2 hours incubation onto several SAMs-coated gold substrates covered by YadC, YadN antibodies, xylose (Xyl), galactose (Gal), lactose (Lac), mannose (Man), or with –OH, –CH₃, –NH₂ and –COOH terminated alkanethiols. ANOVA test was used to compare the differences in the median adhesion values for *E. coli* Δ_4adh_PcLyad and Δ_4adh ; there is a statistically significant difference for * p value < 0.050 (no differences for p value > 0.100).

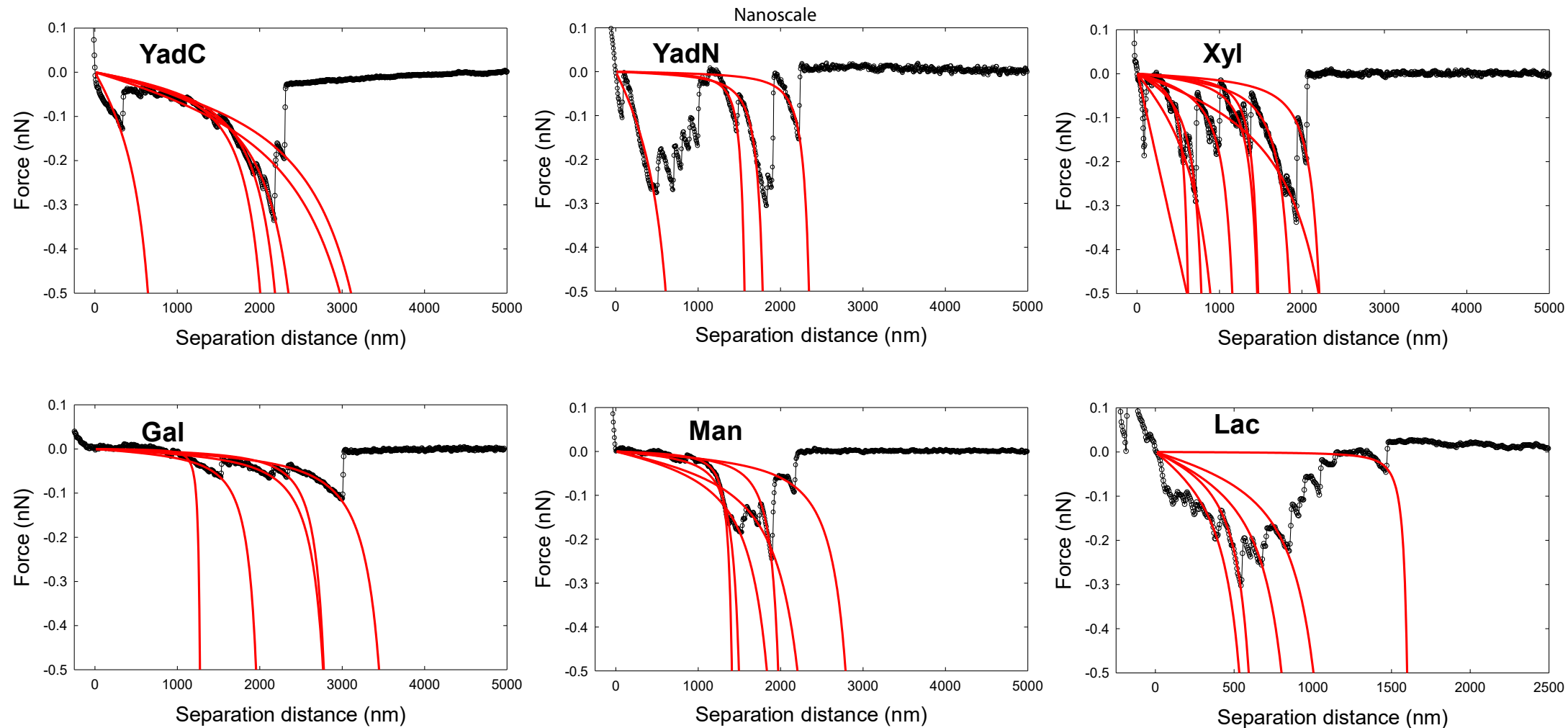


Figure 3 : Illustrative force vs. separation distance profiles (black circles) measured by SMFS upon withdrawal of several AFM-probes (functionalized with YadC, YadN antibodies, xylose (Xyl), galactose (Gal), lactose (Lac) and mannose (Man)) from the cell wall of *E. coli* Δ_4adh_PcLyad . Red lines correspond to theoretical fitting on the basis of the Worm-Like-Chain model (eq 1).

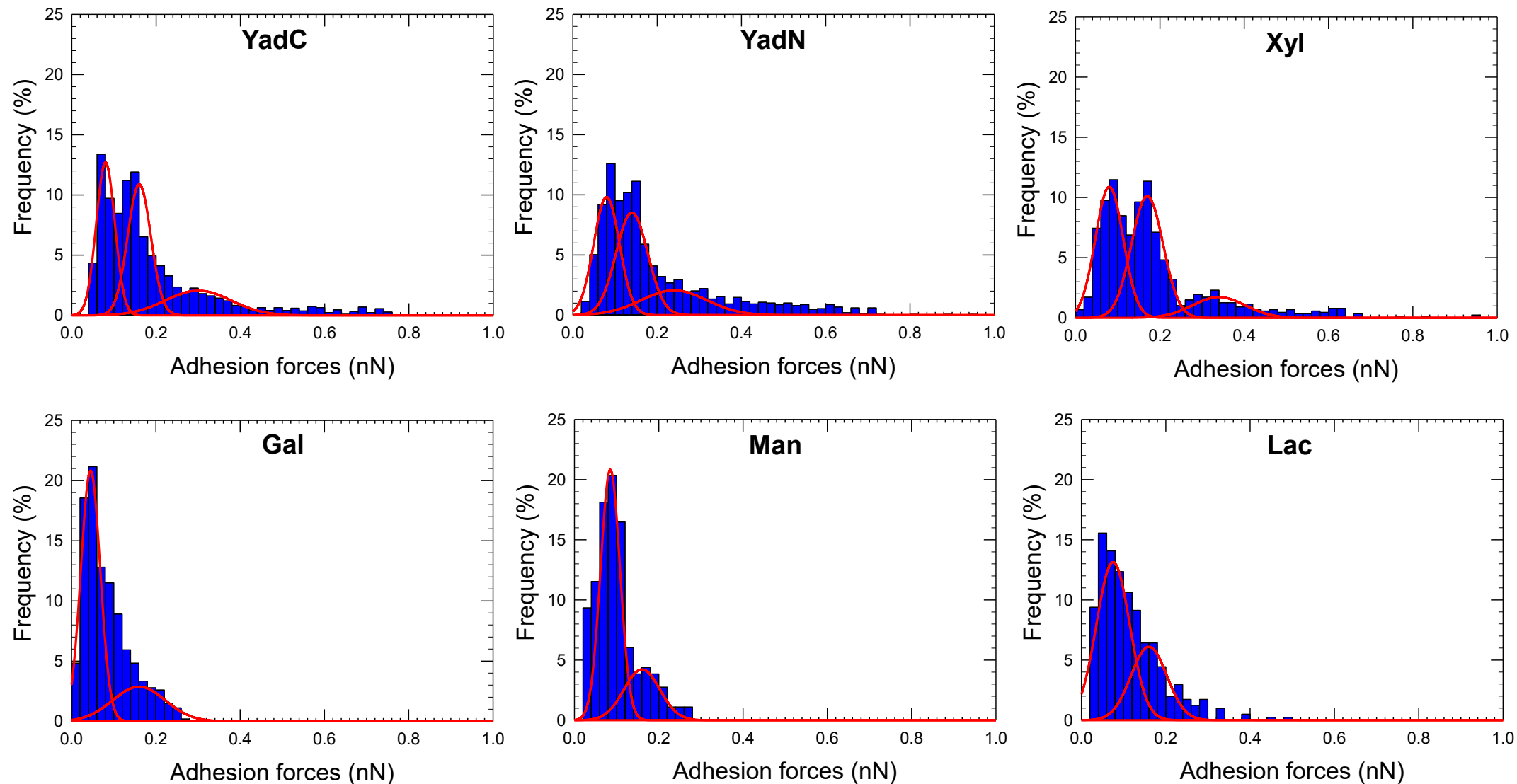


Figure 4 : Statistic distribution of the adhesion forces between *E. coli* Δ_4adh_PcLyad and the different AFM-probes functionalized with YadC, YadN antibodies, xylose (Xyl), galactose (Gal), lactose (Lac) and mannose (Man) (indicated). Red lines correspond to decomposition of the distribution into fundamental Gaussian components.

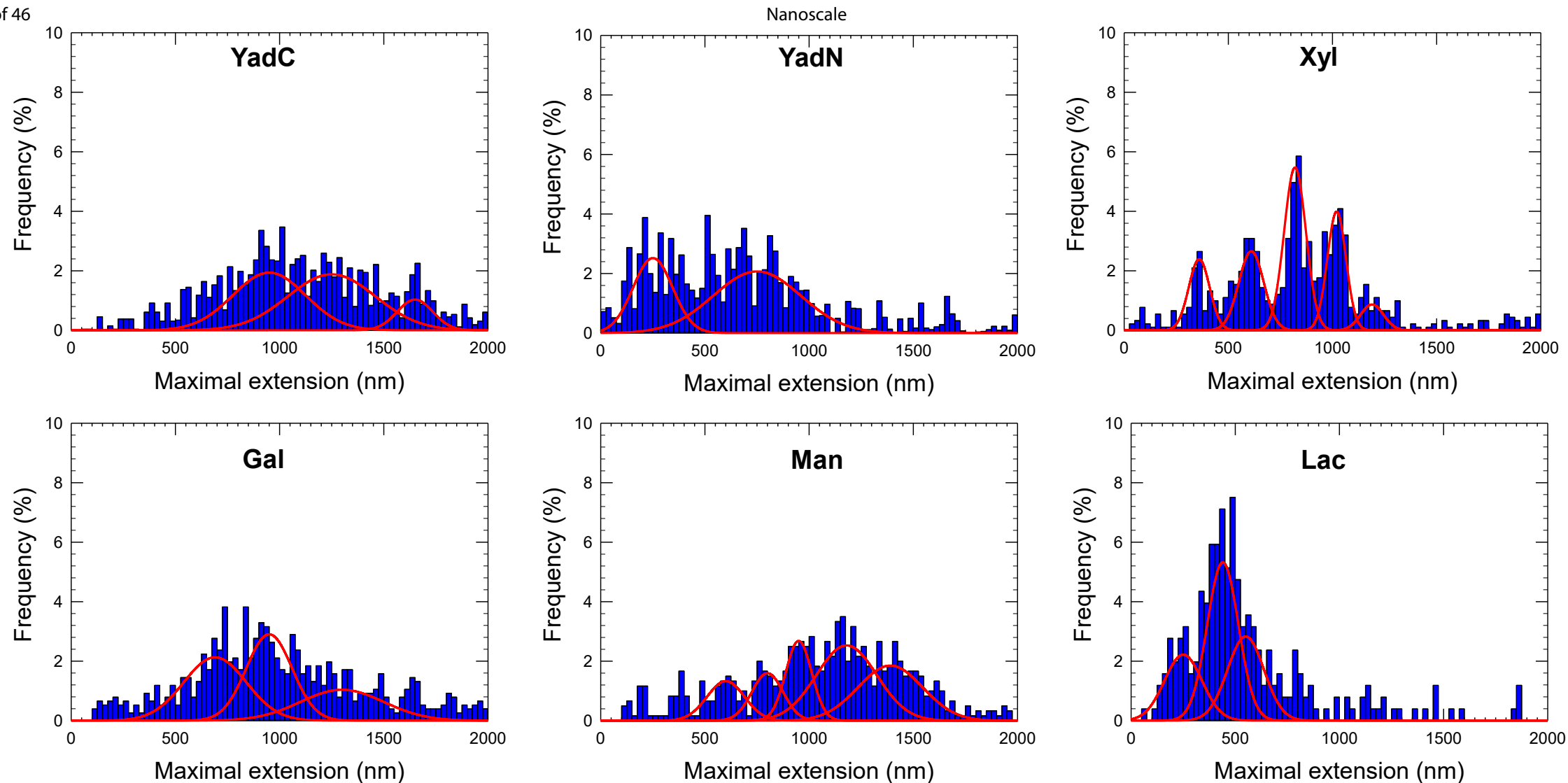


Figure 5 : Statistic distribution of the maximal rupture distances (or maximal Yad fimbriae elongation prior to rupture) estimated from the SMFS force-distance curves measured for *E. coli* Δ_4adh_PcLyad interacting with AFM-probes functionalized with YadC, YadN antibodies, xylose (Xyl), galactose (Gal), lactose (Lac) and mannose (Man) (indicated). Red lines correspond to decomposition of the distribution into fundamental Gaussian components.

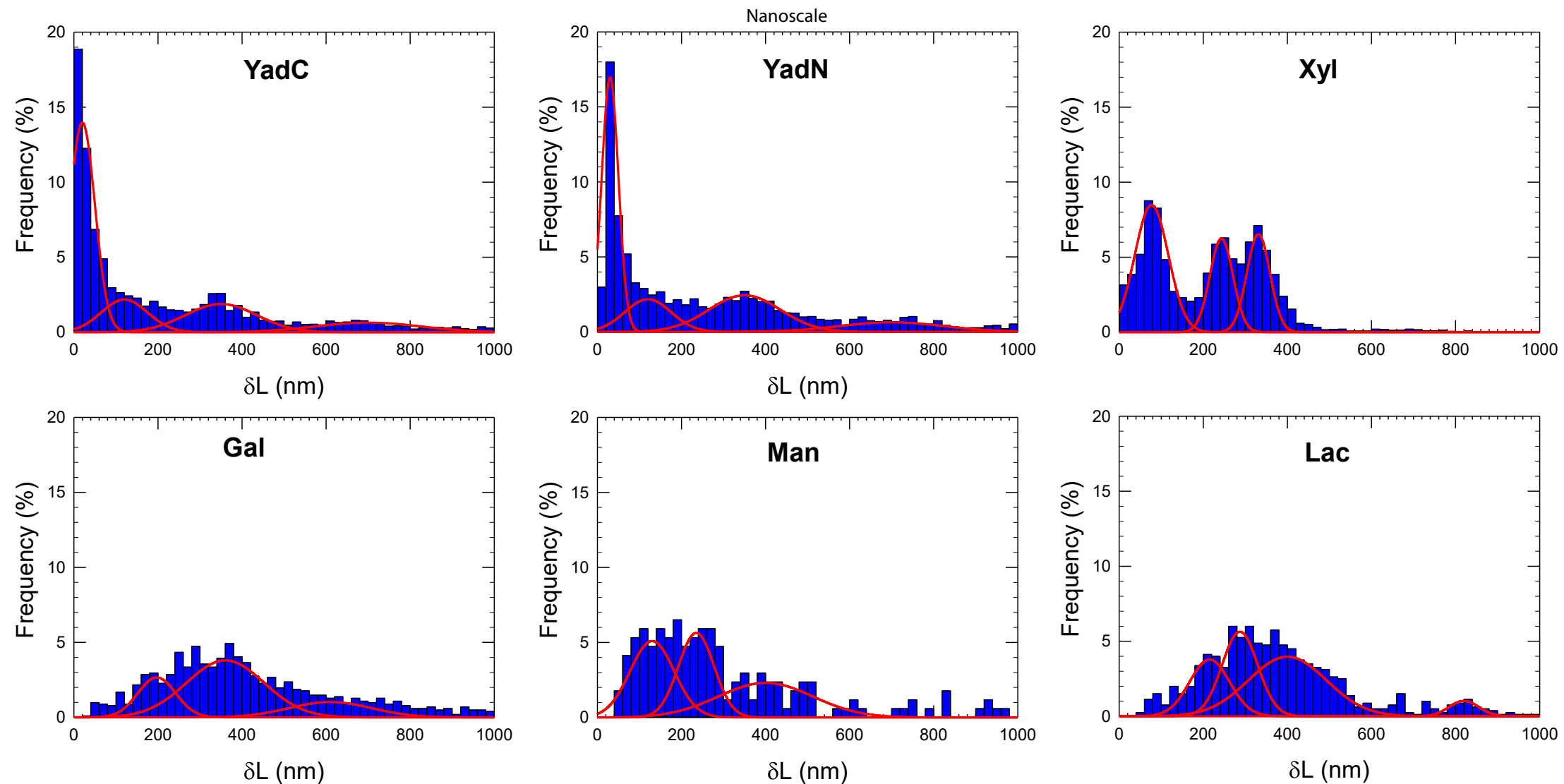


Figure 6 : Statistic distribution of the distance between two successive adhesive events detected on the SMFS force-curves collected for *E. coli* Δ_4adh_PcLyad in interaction with AFM-probes functionalized with YadC, YadN antibodies, xylose (Xyl), galactose (Gal), lactose (Lac) and mannose (Man) (indicated).

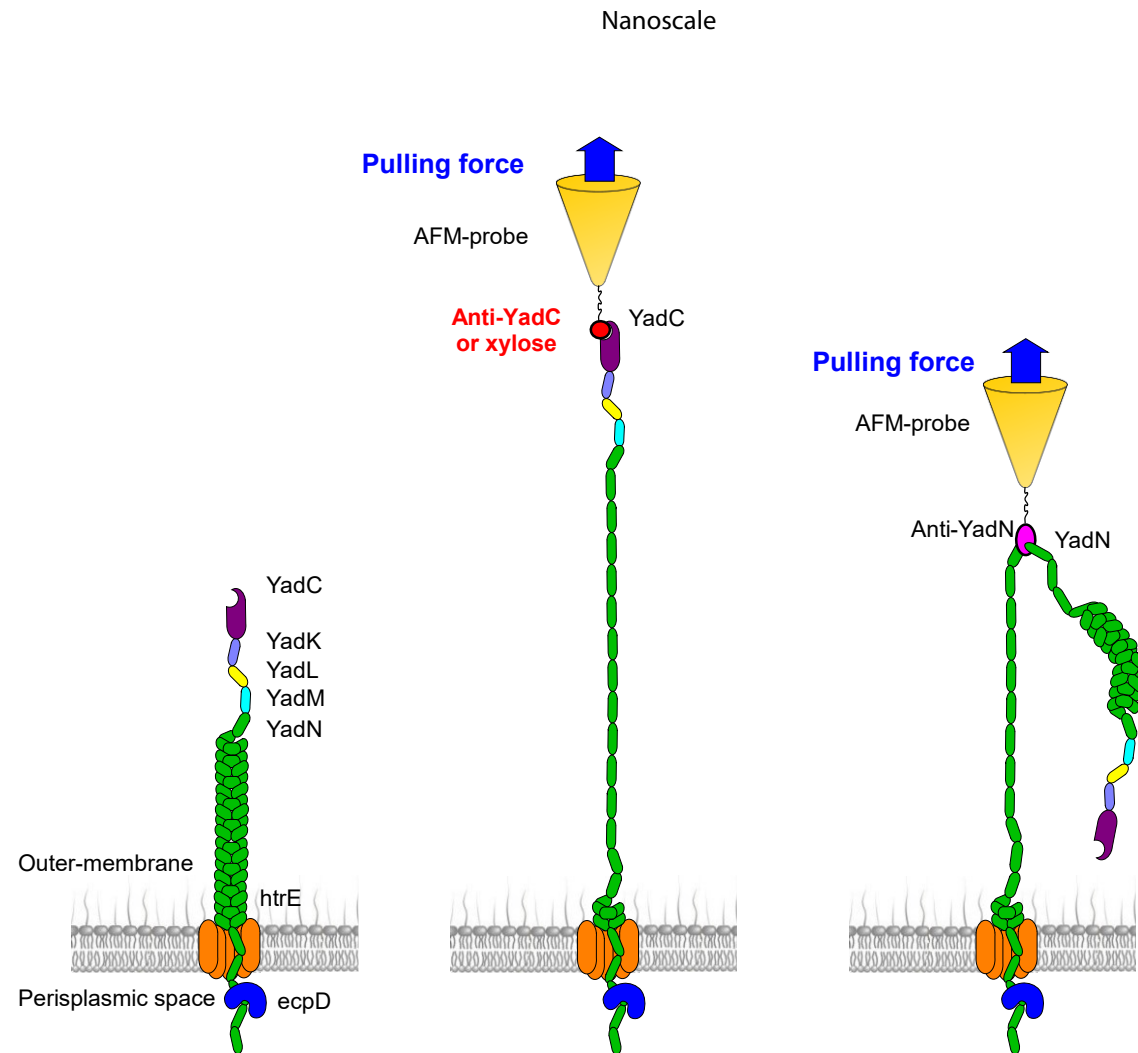


Figure 7 : Schematics for the structure of Yad fimbriae and its possible conformation during stretching by antibodies or xylose residues grafted at the apex of AFM probes.

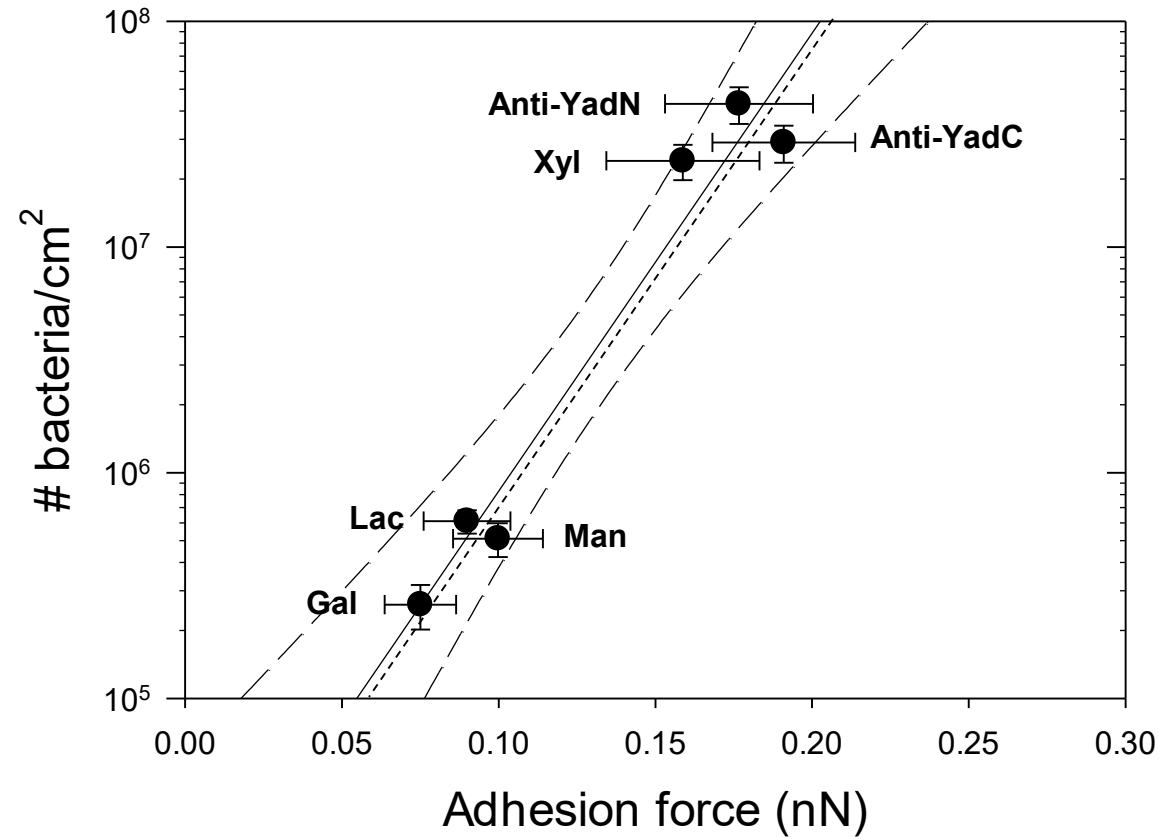


Figure 8 : Dependence of the surface concentration of bacteria adhered onto SAMs-coated gold substrates covered by YadC, YadN antibodies, xylose (Xyl), galactose (Gal), lactose (Lac), mannose (Man) on their corresponding adhesive interactions measured between AFM-probes functionalized with YadC, YadN antibodies, xylose (Xyl), galactose (Gal), lactose (Lac) and mannose (Man)) and individual *E. coli* Δ_4adh_PcLyad . Dashed line corresponds to linear fitting of the data in semi-logarithmic scale.